AEDC-TR-65-169

ARCHIVE COPY
DO NOT LOAN

Cy1
MAR 2 1970

DEVELOPMENT OF THE SUPERSONIC COMPRESSOR TEST FACILITIES AT THE ARNOLD ENGINEERING DEVELOPMENT CENTER

C. T. Carman

ARO, Inc.

This document has been approved for public release
its distribution is unlimited. Per DDC TR-75/5
AD A011 100
Dtd July 1975

October 1965

PROPERTY OF U. S. AIR FORCE
AEDC LIBRARY
AF 40(600)1200

ENGINEERING SUPPORT FACILITY

ARNOLD ENGINEERING DEVELOPMENT CENTER

AIR FORCE SYSTEMS COMMAND

ARNOLD AIR FORCE STATION, TENNESSEE

AEDC TECHNICAL LIBRARY
5 0720 00031 1177

NOTICES

When U. S. Government drawings specifications, or other data are used for any purpose other than a definitely related Government procurement operation, the Government thereby incurs no responsibility nor any obligation whatsoever, and the fact that the Government may have formulated, furnished, or in any way supplied the said drawings, specifications, or other data, is not to be regarded by implication or otherwise, or in any manner licensing the holder or any other person or corporation, or conveying any rights or permission to manufacture, use, or sell any patented invention that may in any way be related thereto.

Qualified users may obtain copies of this report from the Defense Documentation Center.

References to named commercial products in this report are not to be considered in any sense as an endorsement of the product by the United States Air Force or the Government.

DEVELOPMENT OF THE SUPERSONIC COMPRESSOR TEST FACILITIES AT THE ARNOLD ENGINEERING DEVELOPMENT CENTER

C. T. Carman
ARO, Inc.

This document has been approved for public release its distribution is unlimited. Per DDC TR-75-5 AD A011 700 Dt'd July, 1975

AF - AEDC
Arnold AFS Tenn

FOREWORD

The work reported herein was done at the request of Headquarters, Arnold Engineering Development Center (AEDC), Air Force Systems Command (AFSC), under Program Element 61445014, Project 7065, and Task 706501. The results were obtained by ARO, Inc. (a subsidiary of Sverdrup and Parcel, Inc.), contract operator of AEDC, AFSC, Arnold Air Force Station, Tennessee, under Contract AF 40(600)-1200 and under the sponsorship of the Aerospace Research Laboratories (ARL), Office of Aerospace Research (OAR), United States Air Force. The work reported herein was performed under Project 7065, "Aerospace Simulation Techniques Research," for the Fluid Dynamics Facilities Laboratory, under the technical cognizance of 1/Lt Arthur J. Wennerstrom of the ARL. The ARO Project No. was TW2353, and the work was monitored by DCS/Research, Hq AEDC. The research was performed during the period from January 11, 1963 to September 1, 1965. The manuscript was submitted for publication on September 8, 1965.

The technical assistance of Dr. R. A. Kroeger and J. M. Major of ARO, Inc., in performing the dynamic analyses presented in Appendixes I and II is gratefully acknowledged.

This technical report has been reviewed and is approved.

Hans K. Doetsch
Technical Adviser
DCS/Research

Donald R. Eastman, Jr.
DCS/Research

ABSTRACT

The design characteristics, operational capabilities, and instrumentation systems of the supersonic compressor test facilities at AEDC are described and the results of shakedown tests are presented. These facilities consist of (1) a high-speed rotating machine to test 22-in.-diam, single-stage, axial-flow compressor rotors from 5,000 to 17,000 rpm at rotor tip speeds up to 1630 ft/sec and (2) a continuous-flow cascade rig with a 1- by 1.3-in. test section to test the effects of various blade parameters such as area ratio and angle of attack. The primary purpose of these facilities is for further development and evaluation of the concept of blunt-trailing-edge, supersonic compressor blades.

CONTENTS

		Page
	ABSTRACT	iii
I.	INTRODUCTION	1
II.	DESCRIPTION OF THE TEST RIGS	1
III.	INSTRUMENTATION	9
IV.	SHAKEDOWN TESTING	15
	REFERENCES	19
	APPENDIXES -	
	I. CRITICAL SPEED ANALYSIS OF THE HIGH-SPEED DRIVE LINE OF THE SUPERSONIC COMPRESSOR TEST RIG	21
	II. CRITICAL SPEED ANALYSIS OF THE SUPERSONIC COMPRESSOR ROTOR	37

ILLUSTRATIONS

Figure		
1.	Supersonic Compressor Test Rig	53
2.	Compressor Rig Power Requirements	54
3.	Cross-Sectional View of Experimental Compressor	55
4.	Supersonic Compressor Rotor No. 1	56
5.	Mean Radius Profile - Blunt Trailing Edge Blade No. 1	57
6.	Machine Setup for Generating the Blunt Trailing Edge Blading	58
7.	Maximum Centrifugal Stress in the Supersonic Compressor Rotor	59
8.	Cascade Rig Supersonic Compressor Test	60
9.	Cascade Model No. 1 Circular-Arc Blades	61
10.	Cascade Test Rig - Probe Calibration Configuration (Blade Test Setup Shown on Mounting Stand)	62
11.	Details of Instrumentation Stations	63
12.	Details of Cascade Rig Instrumentation	66
13.	Aerodynamic Instrumentation	67
14.	Design Details of Probes	70
15.	Data Processing System Model 123	76
16.	Shadowgraph Apparatus	77

TABLE

I.	COMPRESSOR TEST RIG INSTALLATION	78

SECTION I
INTRODUCTION

Research on supersonic compressor blades conducted by the Aerospace Research Laboratory (ARL), Office of Aerospace Research (OAR), has demonstrated some promising characteristics of a blunt-trailing-edge-type blade. A 5-in.-diam compressor rotor was tested and preliminary results were presented in Ref. 1. Based on the results obtained during that investigation, a program was sponsored at the Arnold Engineering Development Center for the design and construction of large-scale compressor test facilities required for further development and evaluation of the blunt-trailing-edge supersonic compressor blading. These facilities consist of a high-speed rotating machine and a continuous-flow cascade rig.

The rotating machine is designed to test single-stage axial-flow compressor rotors at mechanical speeds varying from 5000 to 17,000 rpm. Maximum tip speed with a 22-in.-diam rotor is 1630 ft/sec at 17,000 rpm.

The cascade rig is designed to evaluate compressor and stator blade configurations over a range of inlet Mach numbers and angles of attack. It may also be used for the calibration of aerodynamic instrumentation.

The purpose of this report is to present the design characteristics and operational capabilities of the compressor and cascade rigs. Details of the aerodynamic and mechanical instrumentation systems are presented. Operational problem areas encountered during shakedown testing are discussed, and the solutions to these problems are described.

SECTION II
DESCRIPTION OF THE TEST RIGS

2.1 COMPRESSOR RIG

A high-speed compressor test rig was constructed to provide facilities for testing 22-in.-diam, single-stage, axial-flow compressor rotors at relative Mach numbers varying from 0.6 to 1.7. A closed-loop configuration was chosen to provide control of the compressor inlet temperature and pressure (Fig. 1). Temperature control of the recirculated air is provided by air-to-water heat exchangers (six F-51

aircraft radiators), and compressor inlet pressure may be varied as desired across the range between 12 and 1.0 psia by an air-driven jet pump. Higher inlet pressures may be obtained by pressurizing the rig before operation. The closed loop also provides protection from damage by foreign objects and contamination by dust, soot, and moisture in addition to increased suppression of the noise generated by the compressor rotor. Testing with working fluids other than air is also feasible with this unit.

It is estimated that the initial compressor will require 2350 hp at design airflow and pressure ratio. These power requirements are provided by an Air Force Model R-4360, air-cooled, reciprocating aircraft engine driving the compressor through a speed increaser gearbox. This engine was modified by removing the reduction gear assembly which had a gear ratio of 0.375:1 and installing a direct drive output shaft. A spacer shaft equipped with suitable gear-type flexible couplings is provided between the engine and the speed-increaser gearbox. The gearbox has a set of double helical gears having an output/input speed ratio of 6.9655. A high-speed, continuously lubricated, crown-gear-type flexible coupling is provided between the gearbox pinion shaft and the compressor torquemeter shaft.

The estimated power requirements of the compressor are compared (in Fig. 2) to the maximum continuous power available from the R-4360 engine (Ref. 2) as functions of engine speed. The estimated requirements for the compressor include 10 percent for mechanical losses in the power train.

An adequate margin of power is available for the operation of the compressor over the entire speed range. Compressors requiring up to 31 percent additional power could be tested in this rig by the installation of a speed increaser gearset with a speed ratio of 6.190:1. This would shift the compressor power curve in the direction of increasing engine speed and utilize the engine power characteristics more efficiently.

The maximum "take-off" power rating of 3500 hp at 2700 rpm with water injection is not shown in Fig. 2 because this power setting is limited to a 5-min duration, which is not an adequate steady-state period for compressor performance testing.

Cooling air for the engine is furnished by a 300-hp, motor-driven, centrifugal fan equipped with variable inlet vanes for airflow control.

Measurement of compressor airflow is accomplished by use of a venturi designed in accordance with the criteria of Ref. 3.

2.1.1 Compressor

The compressor is designed for the evaluation of rotors having a tip diameter of 22 in. and a root diameter of 19.8 in., giving a hub/tip diameter ratio of 0.9. The design tip speed is 1600 ft/sec at 16,680 rpm. Design airflow of the initial compressor is 24 lb/sec at a compressor pressure ratio of 3.7.

A cross-sectional view of the compressor is shown in Fig. 3. Air is guided from the 48-in.-diam inlet plenum (station 1) through a converging annulus between the inlet bell and the bulletnose to the inlet of the blading (station 2). The air passes through the blading into the compressor discharge annulus (station 3) and then into a diverging radial diffuser. The air then flows through the discharge ports of the outer diffuser and throttle valve. The discharge pressure of the compressor is adjusted by circumferentially positioning the ring-type throttle valve.

Compressor rotors having a wide range of physical characteristics might be tested in this machine by modifying or replacing component parts of the compressor. Redesign and replacement of the inner diffuser and the bulletnose would allow the installation of rotors having hub/tip diameter ratios up to 2.0. Replacement of the speed increaser gears with gear sets of different speed ratios would allow testing rotors at different tip speeds.

Initial testing will be performed to determine the performance of the rotor without inlet guide vanes or stators; later testing will be performed with stators and inlet guide vanes. Material has been provided in the inner and outer cases both before and behind the wheel for the installation of stators or guide vanes when required.

A curved quartz window is mounted in the upper compressor case so that shadowgraph pictures may be taken of the shock patterns in the air passing through the wheel. The window is set flush with the inner surface of the compressor case to avoid disturbing the flow through the rotor.

Because of the relatively high axial Mach number of 0.85 at the inlet of the blades, bulletnose support struts could not be tolerated in the constant-area flow passage forward of the rotor. The bulletnose was supported with relatively long struts attached to the outer rim of the inlet bell; however, eight small stabilizing rods were later added between the bulletnose and inlet bell. The compressor rotor was designed to have a cantilevered shaft, thereby avoiding the alignment problems and the additional complications of providing a

bearing, seal, and oil system in the bulletnose that would be required for a simply supported rotor.

A maximum thrust load of 6600 lb occurs at design speed and pressure ratio and acts in the opposite direction to the airflow. A balance piston chamber in the bulletnose could have been used to adsorb this load; however, a balance piston would require very rigid bulletnose supports and an efficient air seal to prevent leakage air from escaping along the face of the wheel and disrupting the airflow into the blading. Therefore, a bearing system was required which would be capable of operating under the following conditions:

Maximum speed	-	17,000 rpm
Maximum thrust load	-	6,600 lb
Radial load	-	300 lb

Pivoted-shoe and fluid-type thrust bearing and journal-type radial bearings were investigated but were not used because of the relatively high cost and more complicated installation and lubrication requirements. Therefore, precision grade, high quality ball bearings were chosen for use in this machine.

The rotor is supported in a heavy, tubular, bearing housing by one light series, 12-deg angular contact bearing located close to the wheel and by two 25-deg, split-inner-race thrust bearings, duplex mounted at approximately three-fourths of the length of the shaft. The torquemeter extension shaft is equipped with a roller-type damper bearing mounted near the midpoint of the shaft.

The front bearing is a Fafnir type No. 2MM9115KMBR. This code number identifies the bearing as having the following characteristics:

2MM - 12 deg angular contact, ABEC-7 tolerances

9115 - single row, extra light, 75MM bore

K - Conrad type, without filling slot

MBR - machined bronze retainer

Material - 52100 nonstabilized bearing steel

This bearing is mounted with a slip fit between the outer race and the bearing housing and is loaded by a wave-washer-type spring to maintain a preload on the thrust bearings.

Bearing life as calculated by the B-10 method is approximately 10,000 hr.

The two split-inner-race thrust bearings are identified by the Fafnir type No. AAMM213-3SMBR-DT and have the following characteristics:

AA - vacuum-melted, stainless steel material

MM - super-precision, ABEC-7 tolerances

213 - single-row, light, 60MM bore

13 - 25-deg angular contact

S - external self-aligning

MBR - machined bronze retainer

DT - duplex tandem mounting

The endurance life of these bearings at design speed and load is calculated to be about 320 hr.

Oil supply passages and drain ports are drilled in the bearing housing. The front bearing and the torquemeter damper bearing are lubricated by oil jets. Lubrication of the thrust bearings is provided by three radial slots machined in each of the mating faces of the outer races. Oil flows from an annular passage around the bearings through these slots and discharges outward through each set of balls. This system ensures equal distribution of oil to each bearing. Synthetic gas turbine oil type TJ-37 is used as the lubricant. This oil is similar to oils conforming to the Military Specification Mil-L-7808C, but has a viscosity value approximately two and one-half times greater with a resulting high load carrying ability.

This machine is designed to incorporate a face-running carbon seal in the bearing housing between the front bearing and the rear face of the rotor to prevent oil leakage into the aerodynamic passages of the compressor. During shakedown testing, it was found that the initial seal design was inadequate; therefore, a balance-chamber labyrinth seal has been installed on a temporary basis while a satisfactory carbon seal is being designed. A balance-chamber labyrinth seal is provided around the high-speed shaft of the gearbox to isolate the compressor oil system from the gearbox and prevent mixing of the synthetic and mineral base lubricants used in the different systems.

An analysis of the dynamic characteristics of the high-speed drive line of the compressor test rig (consisting of the high-speed pinion shaft and torquemeter coupled to the rotor shaft) was performed and is presented in Appendix I. The conclusions determined by this analysis were (1) the critical speed of the high-speed pinion shaft and torquemeter, when coupled together, is approximately 27,730 rpm and (2) the critical torsional speed was predicted to occur at about 6480 rpm.

The critical speed of 27,730 rpm is well above the operating range of the machine. The torsional critical speed is at the low-speed end of the operating range and may be avoided except during transient operation.

The structural portions of the test compressor (inlet bell, bulletnose, compressor casings, diffuser casings, and bearing housing) were cast of Meehanite gray iron, Type G.A., class 50. This material was selected because of its stability and freedom from warpage during machining.

2.1.2 Compressor Rotor

The initial compressor rotor was designed to have the following characteristics:

Airflow	24 lb/sec
Pressure ratio	3.7
Tip diameter	22 in.
Blade height	1.1 in.
Hub/tip ratio	0.9
Chord length	1.563 in.
Blade axial depth	1.105 in.
Inlet angle	60 deg
Number of blades	126
Solidity (chord/pitch)	3
Aspect ratio	0.704
Stagger angle	45 deg
Tip speed (design)	1600 ft/sec

Design relative Mach No. (mid-chord)	1.7
Avg inlet Mach No.	0.85
Rpm, 100 percent	16,680 rpm

This rotor shown in Fig. 4 incorporates the blunt-trailing-edge supersonic blades developed by ARL. The blade profiles represent slender wedges which are curved from the inlet angle of 60 deg to an exit angle of 30 deg. For the first rotor, the blades are segments of circular arcs. The profile and spacing at the mean blade radius are shown in Fig. 5. The sides of the blades are generated by rays originating from the axis of wheel, resulting in a blade that is slightly thicker at the tip than at the root. The blading was machined directly into the rim of the wheel by use of a die mill equipped with a three-dimensional, pantograph-type cam follower, as shown in Fig. 6, which programmed the rotational and axial motions of the rotor and cutterhead to generate the blades.

The cross-sectional profile of the wheel was designed in accordance with the method presented in Ref. 4, section 10-10, in which the rotor disc is designed to have a uniform strength at all radii. This design approach would normally result in a slightly elliptical shape of the rotor sides; however, in this case straight tapered sides were substituted to simplify machining. This change resulted in a stress level at design speed of 54,900 psi at the hub of the wheel which increases to 56,300 psi at a radius of 3 in. and decreases to a value of 33,500 psi at the root of the blades. The stress level at the 3-in. radius (point of maximum stress in the rotor) is presented in Fig. 7 as a function of compressor rotor speed. The integral shaft configuration was chosen to avoid the stress concentration involved in providing mounting holes in the wheels. A critical speed analysis of the compressor rotor and bearing system was also performed and is presented in Appendix II. The critical speed of the shaft and rotor is predicted to occur at approximately 34,100 rpm, well above the operating range. The load on the front bearing at 16,680 rpm with a maximum of 3 gm-in. unbalance was calculated to be 540 lb.

The rotor was fabricated from a one-piece forging made of a vacuum-melted, electric furnace gun steel. This material was specified by the forger to be a Type 4335V alloy equivalent to AISI 4340 steel except for a slightly lower carbon content and the addition of vanadium, thereby allowing the use of a water quench during heat treatment.

The yield strength at 0.2 percent offset was determined by the AEDC Metallurgical Laboratory to be 147,900 psi. The factor of safety for this rotor based on the centrifugal loading and the yield strength is 2.6.

2.2 CASCADE RIG

A continuous-flow cascade rig with a 1- by 1.3-in. test section was constructed to be used for the evaluation of the effects of various blade parameters such as area ratio and angle of attack (Fig. 8). Compressed air from a 4000-psia source is supplied to the cascade rig at 100 to 200 psia through suitable pressure regulators and control valves. Inlet airflow is measured by a small choked-flow venturi. Air flows from the venturi into an inlet plenum which contains pressure equalizing screens and straightening grids. A transition section is provided at the outlet of the plenum to direct the airflow into the rectangular passage of the inlet instrumentation passage where total pressure and temperature data are taken. A one-dimensional nozzle is then provided by the use of contoured nozzle blocks installed in the top and bottom of the passage. Nozzle blocks with various contours are used to vary the blade inlet Mach number from the subsonic range to a maximum of about 1.7.

Blade models are mounted in the test section in such a manner than the angle of attack can be varied while maintaining the position of the model in relation to the centerline of the passage. The first models, such as that shown in Fig. 9, consist of four blades or five flow passages. Boundary-layer flow from the upper and lower walls of the test section is bled off through passages formed by end blades of the model and the walls of rig and is measured with a small venturi. Static pressure measurements are taken upstream of the blades and at the inlets and outlets of three passages. One passage is instrumented to determine the static pressure profile along the passage. Total pressure traverses and flow angle surveys are taken behind the outlets of three passages. Shadowgraph photographs are taken through the observation port at each test condition. Pressure ratio across the blading is adjusted by use of a sliding lattice-type valve.

Development of efficient stator blading has been one of the major obstacles in previous supersonic compressor investigations. This cascade rig is especially suitable for the development of stator blades because the lack of a rotational component in the stator blading allows a more exact simulation of stator inlet flow conditions. In addition, this rig can be used for the calibration of aerodynamic instrumentation probes as shown in Fig. 10.

SECTION III
INSTRUMENTATION

3.1 DETAILS OF INSTRUMENTATION STATIONS

Aerodynamic pressures and/or temperatures are measured at the stations in the compressor shown in Fig. 2. Axial and radial locations and details of the measuring stations in the compressor and at the venturi are shown in Fig. 11. Total and static pressures and total temperatures are measured in straight, constant-area, duct sections to determine airflows, pressure ratio, and efficiency. Traverses of the compressor passages are performed fore and aft of the rotor to determine inlet and exit swirl angles and true stream total pressure. Compressor airflow is measured with a venturi.

Provisions are made at stations 2A, 2B, 3C, 3E, and 3F for mounting a total of four rakes and one traverse actuator per station. Station 3B has provisions for mounting two traverse actuators only. This gives a total of 20 positions for rakes and 7 traverse positions; however, the normal instrumentation consists of four rakes (two total-pressure and two total-temperature) and one angle traverse in front of the rotor; and four rakes (two total-pressure and two total-temperature), one angle traverse, and one combination total-pressure, total temperature traverse behind the rotor. This instrumentation is spread among the various stations as required by the test configurations. The static pressure taps at all stations are always instrumented. The instrumentation layout shown in Fig. 11 is typical for the initial test configuration.

Instrumentation stations in the cascade rig are shown in Fig. 12. Total pressure and temperature are measured upstream of the inlet to the test section nozzle (station 0), static pressure surveys are taken before the blade model, through one passage of the model, and at the discharge of the blades. Total pressure traverses are made at staggered positions across the outlet of three passages. Inlet and boundary-layer bleed airflows are measured with choked-flow venturis similar to those used in the rotating machine. These venturis are instrumented with one wall static tap upstream of the nozzle contour and one static tap at the nozzle throat. Air temperature is assumed to be the same as measured at station 0.

The aerodynamic probes and rakes used in the compressor rig and cascade rig were fabricated by the Instrument Branch

of the Engineering Support Facility (ESF). These probes are shown in Fig. 13 and were designed for the following purposes: (a) conical inlet total pressure rake, for use in the compressor inlet where swirl angles are small; (b) prism-type yaw probe for determining flow angle and total pressure surveys in the compressor inlet passage; (c & d) Kiel-type total-pressure and total-temperature rakes for use in the compressor discharge passage in the presence of large swirl angles; (e) prism-type yaw probe for determining compressor discharge flow angle surveys; and (f) combination total-pressure and total-temperature Kiel probe for traverses across the discharge passage.

Design details of probes "a" through "f" are shown in Fig. 14.

Static taps are drilled at 90 deg with respect to the flow channel axis, and the edges of the orifices are left square. Diameters of the static orifices in the compressor casings are 0.025 in. whereas those in the cascade rig are 0.013 in.

Aerodynamic pressure data are measured by strain-gage transducers, and temperatures are measured by thermocouples. The outputs from these instruments are processed through an analog-to-digital converter and recording system. Air horsepower is calculated from aerodynamic measurements, and mechanical horsepower is measured by a phase shift torquemeter.

Compressor rotor speed is determined by a reluctance-type pickup excited by a 72-tooth gear mounted on the high-speed pinion shaft. The output of this pickup is indicated on a direct-reading frequency counter. Mechanical operating parameters such as oil pressures and temperatures are indicated on Bourdon-type gages and direct-reading millivolt indicators. Table I lists the devices used in measuring and recording the various parameters and the estimated system accuracies.

3.2 INSTRUMENTATION SYSTEMS

3.2.1 Analog-Digital Recording System

The primary data acquisition system in use at the compressor test rig consists of a Beckman Model 123 Data Processing System and accessories shown in Fig. 15. This system is designed to measure and record in digital form the analog outputs of various sensing elements used to determine such values as temperature, pressure, flow, rotational speed, and torque. Steady-state aerodynamic pressure and temperature

data obtained from the compressor rig and the cascade rig are measured and recorded with this system.

3.2.1.1 Method of Operation

The primary function of this system is that of a digital voltmeter in which an input signal is measured and processed, digitally converted, and transferred to the logging section. Scaling and zero offset instructions for each channel are programmed by use of pinboards and diode pins. Logging is accomplished by the following means: (a) Channel Number and Digital Output are displayed in visual readout windows on the face of the cabinet and (b) the Digital Output is typed on log sheets and punched into paper tape by a Flexowriter. This tape is then used as the input data to a digital computer for the calculation of performance parameters.

3.2.1.2 System Specifications

The system accuracies and performance specifications, as listed in Ref. 5, are tabulated below:

Linear Accuracy:

a.	Linear d-c input:	0.05 percent of full-scale rms
b.	System accuracy -- peak to peak measurement:	(1) ±0.2 percent of full scale which equals ±10,000 digits (2) ±10 microvolts (noise) (3) ±1/2-digit digitizing error

Performance:

a.	Channel capacity	100
b.	Scan rate	0.55 seconds per channel
c.	Scan period (100 channels)	1 minute

Readout:

a.	Word length	4 digits plus sign
b.	Full-scale digital range	±10,000
c.	Zero offset digital range	±10,000

Zero offset is pinned in terms of the physical units rather than the analog millivolt input.

3.2.2 Yaw and Traversing Probe System

This system consists of the electronic control circuits necessary to provide manual or automatic control of electromechanical probe actuators in either traverse or angular directions. Linear or angular position is monitored on a rotary indicator. Strip-chart recorders incorporated in the control console record selected parameters, such as flow angle, as a continuous function of probe position.

The probe actuators incorporate a hollow, precision-ground screw through which the probe is inserted and secured by a collet. Motor-driven gear trains impart two motions to the probe and screw. The traverse motion extends and retracts the probe a maximum distance of 2 in. to permit surveying radially with respect to the axis of the test unit. The angular motion rotates the probe a maximum of 180 deg about its own axis to permit the probe head to be aligned for yaw or angular airflow through the unit.

The unbalance sensed by the directional (yaw) probes as they are traversed across the flow passage is applied to the metal diaphragm of a variable-reluctance transducer. The output signal of this transducer is used by the angle balance control to drive the angle probe to a balanced or weather-cocked position. Sensitivity of this transducer is approximately 0.010 psid or less.

This system is capable of operating a maximum of four actuators in sequence by the use of appropriate switching. Calibration and span for each actuator and its specific parameter are set on switchboard-mounted potentiometers before the beginning of test operations.

3.2.3 Torquemeter Description

The compressor rotor is coupled to the high-speed gearbox by a torquemeter extension shaft. This torquemeter was adapted from a design which has been used successfully for several years as a component part of the Air Force Model T56-A-7 turboprop engine. Although the torquemeter was designed to operate at 13,800 rpm, analysis of the dynamic characteristics of the high-speed drive line indicates that it may be operated at speeds well above the compressor design speed of 16,680 rpm.

The rotating portion of the torquemeter is composed of two concentric shafts. The inner shaft, which carries the torsional load, is connected to the outer shaft at the input end only. The forward end of each shaft is flanged. Rectangular exciter teeth are machined in line on the outer

diameters of the flanges. Both shafts rotate as a unit within the torquemeter housing. Two electromagnetic pickups mounted radially over the teeth of the inner and outer shaft flanges produce electrical impulses at the passage of each exciter tooth. The frequencies of these signals are identical and directly proportional to shaft speed. When a load is applied, the torsional deflection of the inner shaft causes a displacement in the alignment between the teeth on the inner flange with respect to the teeth on the outer or reference flange. This change in alignment of the two sets of teeth results in a phase shift between the signals generated by the magnetic pickups which is a linear function of the torque transmitted by the inner shaft. An electronic phase detector converts the phase shift into an electrical signal proportional to torque which is tabulated in inch-pounds by the Beckman system and indicated in the same units on the test operator's panel.

The accuracy and repeatability of the system used in this installation is estimated to be within ±2 percent of the power transmitted at speeds of 10,000 rpm (60 percent) and above. The accuracy of the torquemeter at lower speeds is about ±5 percent.

3.2.4 Shadowgraph System

Shock waves and flow separation in a high-velocity gas stream results in density variations in the gas which may be observed visually by passing parallel light beams perpendicular to the flow and observing the shadow patterns on a screen. The resulting flow patterns observed in the passages of a supersonic compressor may be used in conjunction with measured performance parameters as an aid in the analysis of the performance of the compressor.

The components of the shadowgraph apparatus designed for use in this investigation are shown in Fig. 16. A 2- by 4-1/2-in. curved, constant-thickness quartz window is inleted into the outer compressor casing in the plane of the rotor. Shadowgraphs are obtained by passing light rays approximately radially upon the rotor hub and inner diffuser casing which were painted flat white to serve as a screen. The motion of the rotor is stopped by a stroboscopic spark-gap light source triggered by an electromagnetic pickup which is actuated by a slot in the high-speed gearbox shaft. The input to the spark gap is approximately eight watt-seconds of power with an output of 50 by 10^6 candlepower over a duration of one-half microsecond. The system is energized manually, and the spark gap is timed by the electromagnetic pickup.

A 70-mm camera equipped with 162-mm f/4.5 lens and a remote-controlled film advance is provided.

3.3 CALIBRATION TECHNIQUES

3.3.1 Pressure System

Aerodynamic pressure transducers are subjected to an in-place calibration before the beginning of each test period. Appropriate valving is used to disconnect the pressure transducers from the instrumentation probes and connect them to a known, adjustable, pressure source. The transducers are loaded several times across their rated pressure range to eliminate zero unbalance and residual hysteresis. Regulated pressure is then applied in both ascending and descending directions to settings of approximately 90 percent of the full-scale ratings of the various transducers, and a data scan is recorded at each point. Calibration pressure values are monitored by use of a reference gage which is known to be accurate within ±0.1 percent. At the end of each test period, the rig is vented to atmospheric pressure and a "zero" data scan is recorded and compared to barometric pressure.

3.3.2 Temperature System

An ambient temperature scan of all thermocouples is performed before each test period. At various periods, usually at the beginning and end of a specific series of tests, each aerodynamic thermocouple probe is immersed in a controlled-temperature bath and the observed temperature values are recorded and compared to the bath temperature as measured by a precision thermometer.

3.3.3 Torquemeter

The torquemeter was mechanically calibrated on a dynamometer before the initial installation. During this calibration, the torsional characteristics of the torquemeter shaft were determined and the electronic system was matched to the torquemeter by two calibration adjustments designated as Cal "A" and Cal "B". Before operation, the values of Cal "A" and Cal "B" are checked on the torquemeter readout. Any change in these values from the initial settings are indicative of an electronic malfunction. The mechanical calibration of the torquemeter shaft is constant unless the shaft is stressed beyond the elastic limit.

3.3.4 RPM Counter

The direct-reading frequency counter is electrically calibrated by applying an a-c signal of known frequency to the input of the instrument and observing the indicated value. A rough operational check on the frequency counter can be performed by observing the output of an engine-driven tachometer, multiplying this value by the speed increaser gear ratio, and comparing this value to the counter indications.

SECTION IV
SHAKEDOWN TESTING

The initial phase of shakedown testing consisted of operation of the R-4360 engine and the speed increaser gearbox with the torquemeter shaft and compressor rotor uncoupled. The engine was operated at various speeds from 700 to 2470 rpm which drove the gearbox high-speed shaft at speeds ranging from 4880 to 17,000 rpm.

The starting and operational characteristics of the engine were evaluated, and the mechanical operating parameters of the gearbox (vibration and bearing temperatures) were compared to the values reported in the manufacturer's production test report (Ref. 6). The engine cooling blower was operated, and bearing temperatures and rotor shaft vibration levels were monitored.

The second phase of testing was performed primarily to obtain compressor performance data; however, major operational problems were encountered with the compressor which required specific solutions before performance testing could be completed.

4.1 ENGINE OPERATION

It was anticipated that ignition problems, oil leaks, and other difficulties might be encountered in operating the engine as it had been removed from an excess KC-97 aircraft and had not been run for more than a year. However, after replacing a defective starter motor, the engine started easily and operated satisfactorily. Throttle response was smooth with no tendency to overshoot although the load imposed by gearbox bearing friction and gear windage was quite small.

Engine vibration was monitored by an accelerometer pickup mounted on the reduction gear nose case. Vibration levels during starts went as high as 300 mils displacement; however, steady-state operation averaged about 20 mils. The low-speed couplings and spacer shaft prevent the transmission of the vertical and horizontal components of the engine vibration into the gearbox, but torsional vibration may be transmitted along the drive line.

4.2 SPEED INCREASER GEARBOX

Operation of the gearbox was satisfactory at all points across the speed range except at 92.5 percent of rated speed (15,400 rpm). At this speed, the high-speed pinion shaft

bearing temperatures climbed rapidly, indicating a critical point for the high-speed shaft. Operation at 100 rpm above or below this point was satisfactory.

Bearing temperature data recorded during this period did not correlate well with the values reported in Ref. 6. In general, the high-speed bearing temperatures ran 30 to 50°F above the values recorded during the production test. This difference is attributed to the lack of load on the high-speed shaft because bearing temperature data obtained during subsequent testing with the compressor rotor coupled to the high-speed shaft agreed reasonably well with the production test data.

4.3 ENGINE COOLING BLOWER

Vertical vibration amplitudes in excess of one mil displacement were detected on the shaft and bearing housings of the cooling blower rotor and the armature of the blower drive motor. These vibrations occurred at twice rotational frequency which indicated that some part of the rotation equipment was loose or had excessive clearance. The motor operated smoothly when uncoupled and the blower bearings had been replaced before installation; therefore the floating shaft coupling was disassembled for inspection. The coupling halves were refaced and the gear teeth dressed. This rework reduced the blower vibration to less than 0.5 mil displacement, which was considered satisfactory.

4.4 COMPRESSOR

The compressor was operated across the speed range between 30 to 60 percent of design speed (5000 to 10,000 rpm). Performance data were recorded during these operations but have been found to be invalid because of oil contamination in the aerodynamic passages of the compressor and because of errors and malfunctions in the instrumentation systems.

The major problems encountered during this period and the action taken to correct them are described in the following subsections.

4.4.1 High-Speed Pinion Shaft Seal

Piston-ring-type seals were originally selected for use around the gearbox high-speed pinion shaft to prevent mixing of the different lubricants used in the gearbox and compressor rig bearings. After operation at 40 percent speeds, it was discovered that these seal rings were worn heavily on the side facing the torquemeter housing. Cause of the failure was attributed to improper venting of torquemeter housing

and compressor oil sump which allowed the scavenge oil pump to evacuate this housing to approximately 7 psia. The resulting differential pressure forced the seal rings against one side of the mating grooves, causing increased friction and high wear.

The compressor sumps were vented, and a replacement seal and seal runner were installed; but the wear rate was again excessive. The wear occurred on both sides of this set of rings, apparently because of improper finish in the seal runner grooves.

A balance chamber labyrinth-type seal was designed and installed in place of the piston-ring seals. Operation with this labyrinth-type seal has been satisfactory in operations up to 100 percent speed.

It should be noted that piston-ring-type seals may be satisfactorily used as oil seals in high-speed applications of this type, but care must be taken to avoid placing a pressure differential across the seal.

4.4.2 Bulletnose Vibration

Testing was interrupted during operations at 60 percent speed because of an erratic increase in vibration levels. Inspection of the rotor revealed that the front face of the wheel had rubbed the trailing edge of the bulletnose, causing slight damage to the roots of the blades and front face of the wheel rim. The blade damage was hand blended to remove irregularities, and the remaining discontinuities should not significantly affect the performance of the compressor.

Vibration studies were conducted with an electrodynamic shaker unit to determine the natural frequencies of various parts of the compressor structure. The natural frequency of structural components which may have contributed to the compressor rub are tabulated below:

Inlet bell axial	70 cps
Inlet bell horizontal	15 cps
Inner diffuser horizontal	15 cps
Collector case axial	29 cps

These frequencies are well below any excitation encountered during normal operation. However, subsequent testing revealed that 70 cps corresponds closely to the surge frequencies encountered in the 40 to 50 percent speed range.

Oscillograph traces recorded from an accelerometer mounted on the bulletnose showed an axial displacement during surge of 0.070 in. This displacement was sufficient to allow the bulletnose to strike the wheel.

A rub ring was fabricated of cloth-base, phenolic-impregnated plastic and installed on the trailing edge of the bulletnose. Six 0.40-in.-diam tie bolts were installed through the inlet bell and bulletnose at a location where the velocity in the inlet passage does not exceed Mach 0.3. In addition, the effective length of the main bulletnose support struts was decreased from 48 to 40.5 in. (about 15 percent by bolting the strut to the flat face portion of the inlet bell). This extra restraint raised the resonant frequency of the inlet bell-bulletnose assembly to a level of about 130 cps and allows only very small displacements.

During performance testing, the innermost inlet thermocouples indicated that the air next to the bulletnose was 4 to 5°F hotter than the air flowing along the outer wall. It was apparent that air trapped in the bulletnose was adsorbing considerable windage work because of friction with the face of the wheel. A diaphragm was installed in the bulletnose close to the face of the wheel. Later testing showed that the temperature gradient between the air along the inner and outer walls of the inlet annulus had dropped to about 1°F.

4.4.3 Rotor Balance

During operations at 50 and 60 percent speeds, the front compressor bearing thermocouples had indicated 200 to 225°F. This temperature was considered excessive, and unbalance of the compressor rotor was suspected to be the cause. Upon disassembly of the machine for modification of the bulletnose, the rotor was taken to a jet engine overhaul facility for balancing. Corrections of 90 gm-in. in the plane of the wheel and 14 gm-in. in the plane of the coupling were required.

The rotor had been subjected to a balance check during manufacture; however, the subcontractor's equipment apparently lacked the necessary sensitivity to detect this unbalance.

4.4.4 Compressor Air-Oil Seal Leakage

Upon removal of the compressor rotor for balancing, it was found that an oil leak had occurred in the region of the compressor shaft carbon seal. It is not possible to inspect this seal without uncoupling the rotor and moving the rotor and bearing housing out of the inner diffuser; therefore, it

was difficult to determine whether the oil was actually leaking through or around the seal. Investigation revealed that the oil was leaking between the carbon face and the seal mating ring at speeds as low as 7000 rpm even though the seal faces and installation were within design requirements. Consultation with the seal manufacturer revealed the fact that centrifugal oil loads on the face of the seal (about 95 psid at 16,680 rpm) had not been considered in the design.

A balance-chamber labyrinth seal was designed and installed in place of the carbon seal. Although the labyrinth seal stopped the oil leakage, the use of this type of seal is considered to be a temporary solution, and efforts will be made to arrive at a satisfactory carbon seal design.

REFERENCES

1. Johnson, E. G., Von Ohain, H., Lawson, M. O., and Cramer, K. R. "A Blunt Trailing Edge Supersonic Compressor Blading." WADC-TN-59-269, August 1959.

2. Model Specification No. A-7091-G, Engines, Aircraft R-4360-59B Pratt and Whitney Aircraft, Division of United Aircraft Corporation, East Hartford, Conn., July 7, 1953.

3. Smith, R. E., Jr. and Matz, R. J. "Verification of a Theoretical Method of Determining Discharge Coefficients for Venturis Operating at Critical Flow Conditions." AEDC-TR-61-8, September 1961.

4. Jennings, Burgess H. and Rogers, Williard L. "Gas Turbine Analysis and Practice." McGraw-Hill Book Company, Inc., New York, 1953.

5. Instruction Manual No. 50028, Beckman Systems Data Processing System Model 123, Systems Division, Beckman Instruments, Inc., Anaheim, California, May 1959.

6. Messmer, G. A. "Production Test Report, Model 160HS80, Serial 111, S. O. 129-80085." Western Gear Corporation, Belmont, California, January 21, 1964.

APPENDIX I
CRITICAL SPEED ANALYSIS OF THE HIGH-SPEED DRIVE LINE OF THE SUPERSONIC COMPRESSOR TEST RIG

INTRODUCTION

This calculation contains a critical speed analysis of the high-speed pinion and shaft, and the midbearing torquemeter in the supersonic compressor system. These components are considered individually and as an assembly in this analysis.

CONCLUSIONS

The following items were found:

1. The critical speed of the torquemeter lies between 13,610 and 19,450 rpm.

2. The critical speed of the high-speed pinion and shaft, and the midbearing torquemeter, when coupled together is approximately 27,730 rpm. This is considerably above the operating range.

3. The critical torsional speed was found to be about 6480 rpm.

DISCUSSION

This analysis was performed to determine the presence of any critical rotational speeds of a supersonic test compressor system within its normal operational speed range. Under such a condition, only the lower limit of the critical frequencies was found.

The system under consideration lent itself to considerable simplifications. Thus the results should be construed only as qualitative.

The midbearing torquemeter was first considered. For its first mode the critical frequency was determined to lie between 13,610 and 19,450 rpm. The operating speed of the compressor lies within this range. However, the torquemeter assembly contains a damper bearing located slightly away from the midspan of the torquemeter shafts. This would of course eliminate the first mode danger. The upper and lower limits for the second mode were both much higher than the maximum operational speed.

The assembly of the torquemeter and the high-speed pinion and shaft was then considered. The natural frequency for this arrangement was found to be about 27,700 rpm which is well above the operating speed.

The assumptions made in the analysis are shown in the computations along with diagrams of the analytical models used.

The critical torsional speed was found to be approximately 6480 rpm which corresponds to 930 engine rpm. Extended operation at this speed, however, can be avoided since it lies below the normal testing range of 40 to 100 percent speed. In any case, the engine speed should be maintained at 950 rpm or above. Another important consideration is that the polar moment of inertia used for the engine is very conservative. This means that the critical speed would be less than 900 if the moment of inertia was increased.

DESCRIPTION OF SYSTEM

The following dimensions and properties were obtained from the References given at the end of this appendix.

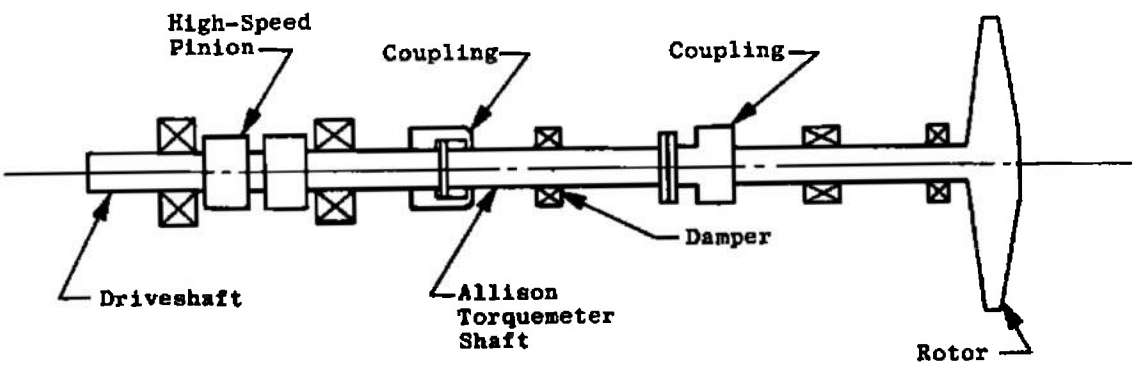

Fig. I-1

Consider the torquemeter:

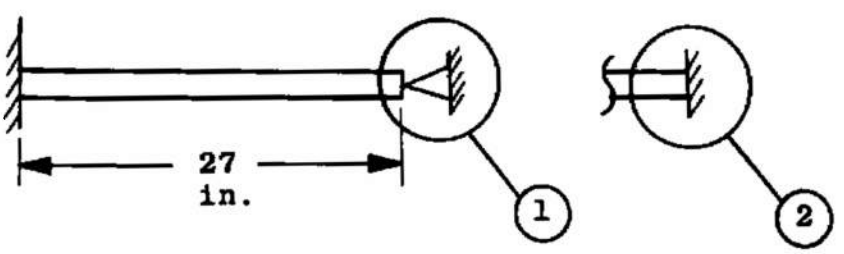

Fig. I-2

Inner shaft:

$E = 30 \times 10^6$ psi

$d = 1.41$ in.

$I = \frac{\pi d^4}{64} = 0.1943$ in.^{4}: $EI = 5.829 \times 10^6$

$W = 13.353$ lb $\quad \ell = 27$ in.

$w = 0.4946$ lb/in.

$\mu = \frac{\omega}{g_c} = 0.001281$

$$\sqrt{\frac{EI}{\mu \ell^4}} = \sqrt{\frac{5.829 \times 10^6}{(0.001281)(27)^4}} = \sqrt{0.85624 \times 10^4} = 0.92533 \times 10^2$$

Condition 1 (Fig. I-2):

$a_1 = 15.4$

$$\omega_N = a_N \sqrt{\frac{EI}{\mu_1 \ell^4}}$$

Ref.: Den Hartog, J. P. Mechanical Vibrations, Eq. (29) p. 432. (Fourth Edition)

$\omega_1 = 15.4(0.92533 \times 10^2) = 1425$ rad/sec

$\omega_2 = a_2(0.92533 \times 10^2) = 50(92.533) = 4627$ rad/sec

$f_1 = \frac{60}{2\pi} \omega_1$ rpm $= 9.55(1425) = 13{,}610$ rpm

$f_2 = 9.55\ \omega_2 = 9.55(4627) = 44{,}188$ rpm

Condition 2 (Fig. I-2):

$a_1 = 22 \quad f_1 = \frac{22.0}{15.4}(13{,}610) = 19{,}448$ rpm

$a_2 = 61.7 \quad f_2 = \frac{61.7}{50}(44{,}188) = 54{,}528$ rpm

Conclusion I: If inner shaft is as shown in the Allison Div. Dwg. AL14267, f_1 lies between 13,610 rpm (for fixed-pinned end condition) and 19,448 rpm (fixed-fixed end condition).

Consider Effect of Outer Torquemeter Shaft:

Assuming the inner shaft lies on the outer shaft, which would be the worst case, the expression

$$\sqrt{\frac{EI}{\mu \ell^4}}$$

is much larger than for the first case. Thus, this is not the critical condition.

Consider now the driveshaft

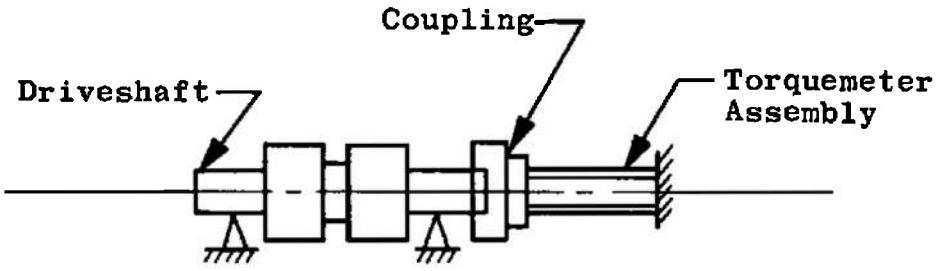

Fig. I-3

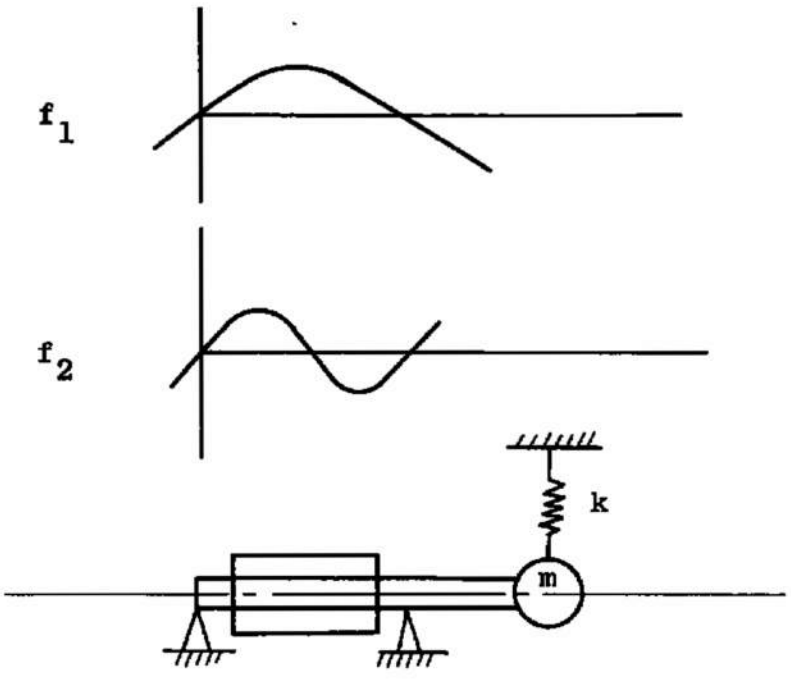

Fig. I-4
Analytical Model

Assumptions:

(1) The shaft between the bearing is infinitely stiff.

(2) The critical condition is when the inner torquemeter shaft is pinned (including the coupling) to the driveshaft.

With these assumptions, our analytical model now becomes:

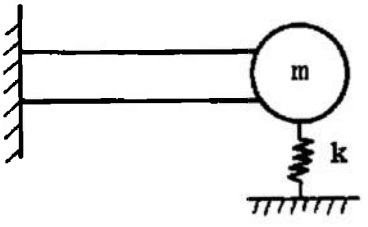

Fig. I-5

Solution of k:

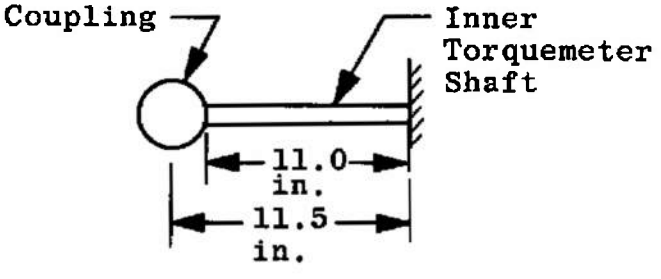

Fig. I-6

(1) Find ω_1

(2) Find k_o

(3) Use equivalent system and find $m_{effective}$

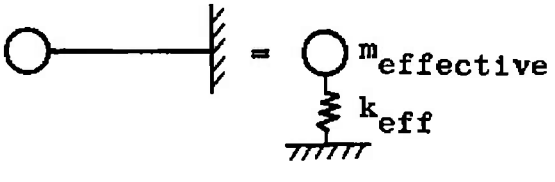

Fig. I-7

(1) $\mu = 0.001281$

$EI = 5.829 \times 10^6$

$\ell = 11.0$ in.

$$\sqrt{\frac{EI}{\mu \ell^4}} = \sqrt{\frac{5.829 \times 10^6}{(0.001281)(11.0)^4}} = 557.49$$

$a_1 = 3.52$ (for cantilever, Fig. I-6)

$\omega_1 = 3.52\ (557.49) = 1962.4$ rad/sec

$$k_{effective} = \frac{3EI}{\ell^3} = \frac{(3)(5.829)(10^6)}{(11.0)^3} = 1.3138 \times 10^4$$

Mass of Cantilevered Mass
(See Ref. Dwg. CC-24462)

A_i	x	ℓ_i	x	2π	= V_i
(1.492 x 0.258)	x	0.895	x	6.2832	= 3.4450
(0.25 x 0.35)	x	1.225	x		= 0.6735
(0.2 x 0.55)	x	1.655	x		= 1.1440
(0.1 x 0.3)	x	1.5	x		= 0.2827
					Vol = 5.545 in.^{3}

$\varphi = 0.29$ lb/in.^{3}

$$m = \frac{0.29(5.545)}{386} = 0.0041659$$

$$\omega_2 = \sqrt{\frac{k}{m}} = \left(\sqrt{\frac{1.3138}{0.0041659}}\right) 10^2 = 1776 \text{ rad/sec}$$

By Dunkerly's Equation:

$$\frac{1}{\omega_c^2} = \frac{1}{\omega_1^2} + \frac{1}{\omega_2^2} = \frac{1}{(1962.4)^2} + \frac{1}{(1776)^2}$$

$$= 2.5967 \times 10^{-7} + 3.1704 \times 10^{-7} = 5.7671 \times 10^{-7}$$

$$\sqrt{\omega_c^{\,2}} = \omega_c = \sqrt{\frac{1}{5.7671 \times 10^{-7}}} = \sqrt{1.734 \times 10^6}$$

$$\omega_c = 1317 \text{ rad/sec}$$

Approximate mass of system (Fig. I-7) attached to drive:

Assume one-third of mass of overhung beam plus mass of the beam end.

$$W = \frac{1}{3}\left(\frac{11}{27} \times 13.353\right) + 0.29(5.545)$$

$$= 1.8133 + 1.608 = 3.4213 \text{ lb}$$

$$m_{effective} = \frac{3.4213}{386} = 0.0088635 \text{ snails}$$

$\therefore$ Since $\omega_N^{\,2} = (1.734 \times 10^6)$ and $\omega_N^{\,2} = \dfrac{k_{eff}}{m_{eff}}$

$$k_{effective} = \omega_N^{\,2}\, m_{eff}$$

$$= (1.734 \times 10^6)(0.0088635)$$

$$= 1.5369 \times 10^4 \text{ lb/in.}$$

Mass of coupling minus mass of coupling on torquemeter end:

$$W_{c-E} = 14.0 - (0.29)(5.545) = 12.39 \text{ lb}$$

$$m_{c-E} = \frac{12.39}{386} = 0.0321 \text{ snails}$$

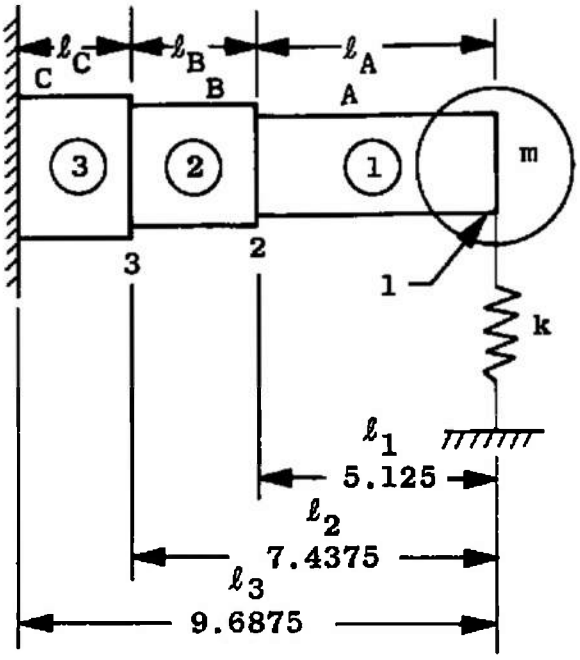

This is detail of Fig. I-5.

ℓ_A = 5.125 in.
ℓ_B = 2.3125 in.
ℓ_C = 2.250 in.

Diam
(1) = 3.125 in.
(2) = 3.250 in.
(3) = 3.370 in.

We are assuming the mass m to be concentrated 1 in. from the end of the driveshaft overhang.

$$I = \frac{\pi D^4}{64} = 0.04908\ D^4$$

I_1 = 4.68063 in.^{4}
I_2 = 5.47568 in.^{4}
I_3 = 6.33030 in.^{4}

Find the stiffness at - 1 - (or find k).

First calculate the influence coefficient a_{11}:

with a 1-lb load at - 1 -,

$$a_{11} = \Delta_1 + \Delta_2 + \Delta_3 + \theta_2 \ell_1 + \theta_3 \ell_2 \longleftarrow$$

where

$$\Delta_1 = \frac{\ell_A^{\ 3}}{3EI_A}$$

$$\Delta_2 = \frac{\ell_B^{\,3}}{3EI_B} + \frac{\ell_B^{\,2}(\ell_1)}{2EI_B}$$

$$\Delta_3 = \frac{\ell_C^{\,3}}{3EI_C} + \frac{\ell_C^{\,2}(\ell_2)}{2EI_C}$$

$$\theta_2\ell_1 = \ell_1\left[\frac{\ell_B^{\,2}}{2EI_B} + \frac{\ell_1\ell_B}{EI_B}\right]$$

$$\theta_3\ell_2 = \ell_2\left[\frac{\ell_C^{\,2}}{2EI_C} + \frac{\ell_2\ell_C}{EI_C}\right]$$

$$\Delta_1 = \frac{1}{E}\left[\frac{\ell_A^{\,3}}{3I_A}\right] = \frac{1}{E}\left[\frac{(5.125)^3}{3(4.68063)}\right] = \frac{9.5864}{E}$$

$$\Delta_2 = \frac{1}{E}\left[\frac{(2.3125)^3}{3(5.47568)} + \frac{(2.3125)^2(5.125)}{2(5.47568)}\right] = \frac{1.2411}{E}$$

$$\Delta_3 = \frac{1}{E}\left[\frac{(2.25)^3}{3(6.3303)} + \frac{(2.25)^2(7.4375)}{2(6.3303)}\right] = \frac{3.5738}{E}$$

$$\theta_2\ell_1 = \frac{1}{E}\left[\frac{(5.1250)(2.3125)^2}{2(5.47568)} + \frac{(5.1250)^2(2.3125)}{5.47568}\right] = \frac{13.5952}{E}$$

$$\theta_3\ell_2 = \frac{1}{E}\left[\frac{(7.4375)(2.25)^2}{12.6606} + \frac{(7.4375)^2(2.25)}{6.3303}\right] = \frac{22.6353}{E}$$

$$\Sigma = a_{11} = \frac{50.6318}{E} \longleftarrow$$

Consider shear deflection:

Ref.: Roark, R. J. Formulas for Stress and Strain, p. 120. (Third Edition)

$$y_s = F \frac{P\ell}{AG} \quad \text{Cantilever, end load P}$$

$$F = \frac{10}{9} \text{ (For solid circular section)}$$

$$G = E/2(1 + v) = E/2.6$$

$$A = \frac{\pi d^2}{4}$$

$$\therefore \quad y_s = \frac{26P\ell}{9AE} = 2.89 \frac{P\ell}{AE}$$

For 1-lb load:

$$y_s = \frac{2.89}{E} \left[\frac{\ell_A}{A_1} + \frac{\ell_B}{A_2} + \frac{\ell_C}{A_3}\right]$$

$$= \frac{2.89}{E} \left(\frac{4}{\pi}\right) \left[\frac{\ell_A}{D_1^2} + \frac{\ell_B}{D_2^2} + \frac{\ell_C}{D_3^2}\right]$$

$$= \frac{3.68}{E} \left[\frac{5.125}{3.125^2} + \frac{2.3125}{3.25^2} + \frac{2.25}{3.37^2}\right]$$

$$= \frac{3.68}{E} (0.9418) = \frac{3.465}{E}$$

$$\delta_{11_{shear}} = \frac{3.465}{E}$$

∴ Including shear

$$a_{11} = \frac{1}{E} (54.0968)$$

so

$$K_{11} = \frac{E}{54.0968} = \frac{30 \times 10^6}{54.0968} = 0.55456 \times 10^6$$

If

$$\Delta = \frac{P\ell^3}{3EI} \text{ then } (EI)_{equiv} = \frac{\ell^3}{3\Delta_{1^\#}} = \frac{\ell^3}{3a_{11}} = \frac{k_{11}\ell^3}{3}$$

$$(EI)_{equiv} = \frac{(9.6875)^3(0.55456 \times 10^6)}{3} = 168.05925 \times 10^6$$

Volume of driveshaft: $\ell \times \frac{\pi D^2}{4} \times \frac{\varphi}{g}$

D	D^2	ℓ	ℓD^2	$\ell D^2\ \varphi/g$
3.125	9.7656	5.125	50.0487	0.029534
3.250	10.5625	2.3125	24.4258	0.014414
3.370	11.3569	2.250	25.553	0.015079
				0.059027

$$\mu = \frac{0.059021}{9.6875} = 0.0060931$$

$$\omega_1 = 3.52 \sqrt{\frac{(EI)_{equiv}}{\mu\ell^4}} = 3.52 \sqrt{\frac{168.05925}{0.0060931 \times (9.6875)^4}} \times 10^3$$

$$\omega_1 = 3.52 \sqrt{3.13169} \times 10^3 = 3.52(1.76965 \times 10^3)$$

$$\omega_1 = 6.22918 \times 10^3$$

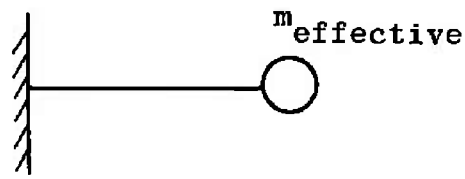

$$\omega_N^2 = \frac{k_{eff}}{m_{eff}} \quad \therefore \quad m_{eff} = \frac{k_{eff}}{\omega_N^2}$$

$$m_{eff} = \frac{0.55456 \times 10^6}{38.8029 \times 10^6} = 0.01429$$

Thus the equivalent mass at (1) becomes:

0.0142917	Shaft
0.0088635	End Plus Torquemeter
0.0321000	Coupling - End
0.0552552	snails

k becomes:

55.456×10^4	(Shaft)
1.3138×10^4	(Torquemeter)
56.7698×10^4	

$$\omega_N = \sqrt{\frac{k}{m}} = \sqrt{\frac{56.7698}{0.055255}} \times 10^2 = \sqrt{1027.4} \times 10^2$$

$$\omega_N = 3205.33 \text{ rad/sec} = 30{,}610 \text{ rpm}$$

Including the mass of the "seal runner", the total equivalent mass at (1) becomes:

0.0142917	Shaft
0.0088635	End Plus Torquemeter
0.0321000	Coupling Minus End
0.0120620	Seal Runner (4 lb 10-1/2 oz)
0.0673172	snails

k becomes:

$$k_{total} = \begin{array}{r} 55.456 \times 10^4 \\ 1.3138 \times 10^4 \\ \hline 56.7698 \times 10^4 \end{array}$$

$$\omega_N = \sqrt{\frac{k}{m}} = \sqrt{\frac{56.7698}{0.067317}} \times 10^2$$

$$= \sqrt{843.32} \times 10^2$$

$$\omega_N = 2903.93 \text{ rad/sec}$$

$$\omega_N = 27{,}730 \text{ rpm}$$

Consider the torsional critical frequency:

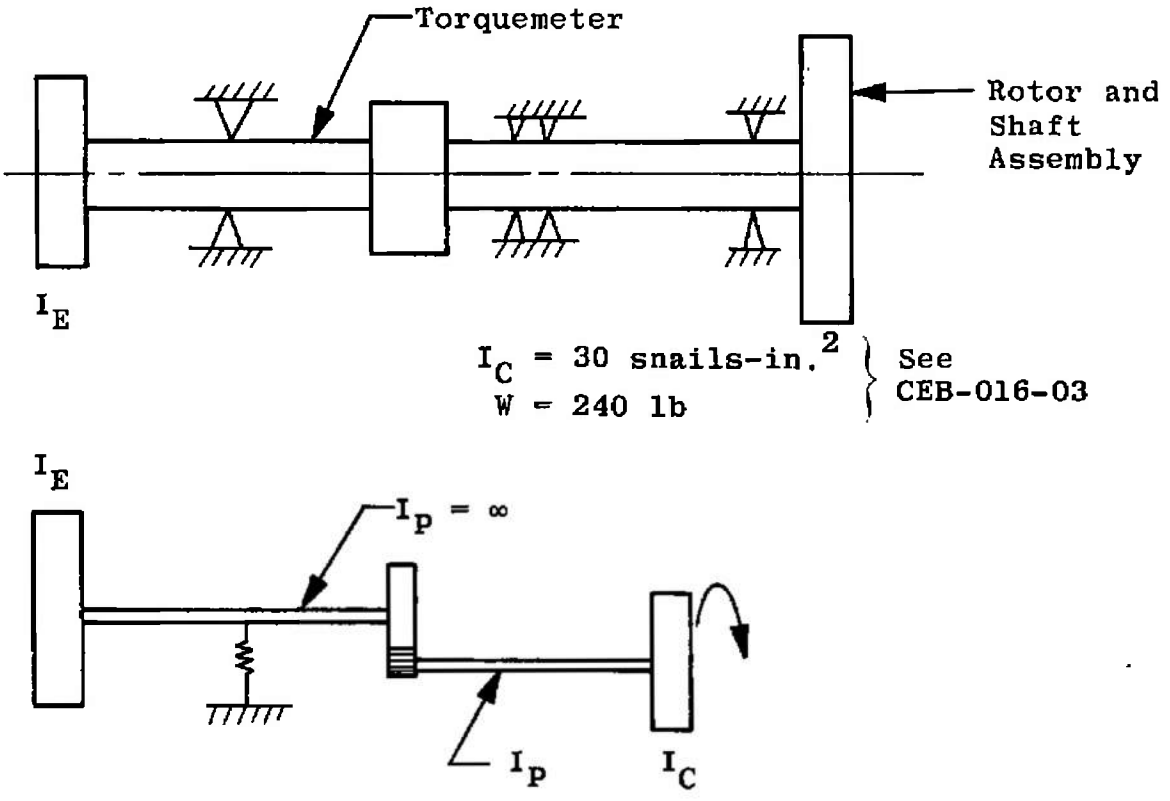

Analytical Model

$$I_C = 30 \text{ snails-in.}^2$$

$$I_E = 1.665 \text{ slugs-ft}^2 \times \frac{144}{12} = 19.98 \text{ snails-in.}^2$$

$$\eta = 6.9655 \text{ (Gear ratio)}$$

$$I_{\text{eff engine}} = \frac{19.98}{(6.9655)^2} = 0.4118$$

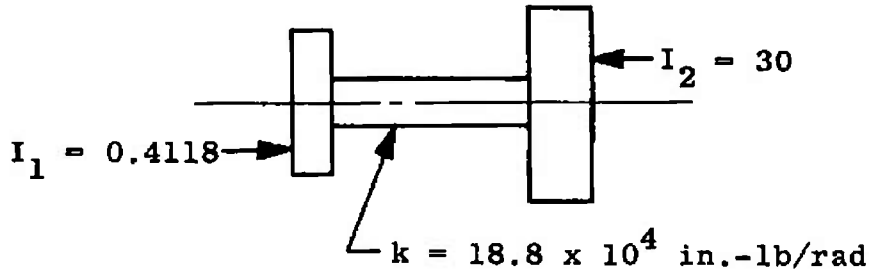

$$\omega_N = \sqrt{\frac{k(I_1 + I_2)}{I_1 I_2}} = \sqrt{\frac{18.8 \times (30.4118)}{12.354}} \times 10^2$$

$$= \sqrt{46.29} \times 10^2$$

$$\omega_N = 680.4 \text{ rad/sec} \quad \therefore \; f = 6498 \text{ rpm}$$

Engine torque input:

$N = 2400$ rpm (max)

$$f = 14 \frac{\text{cylinders}}{\text{cycle}} \times 2400 \frac{\text{cycle}}{\text{min}} = 33{,}600 \frac{\text{cylinder firings}}{\text{min}}$$

for $f = 6498$ rpm

Engine speed $N = \dfrac{6498}{16{,}800} \times 2400 = 930$ rpm

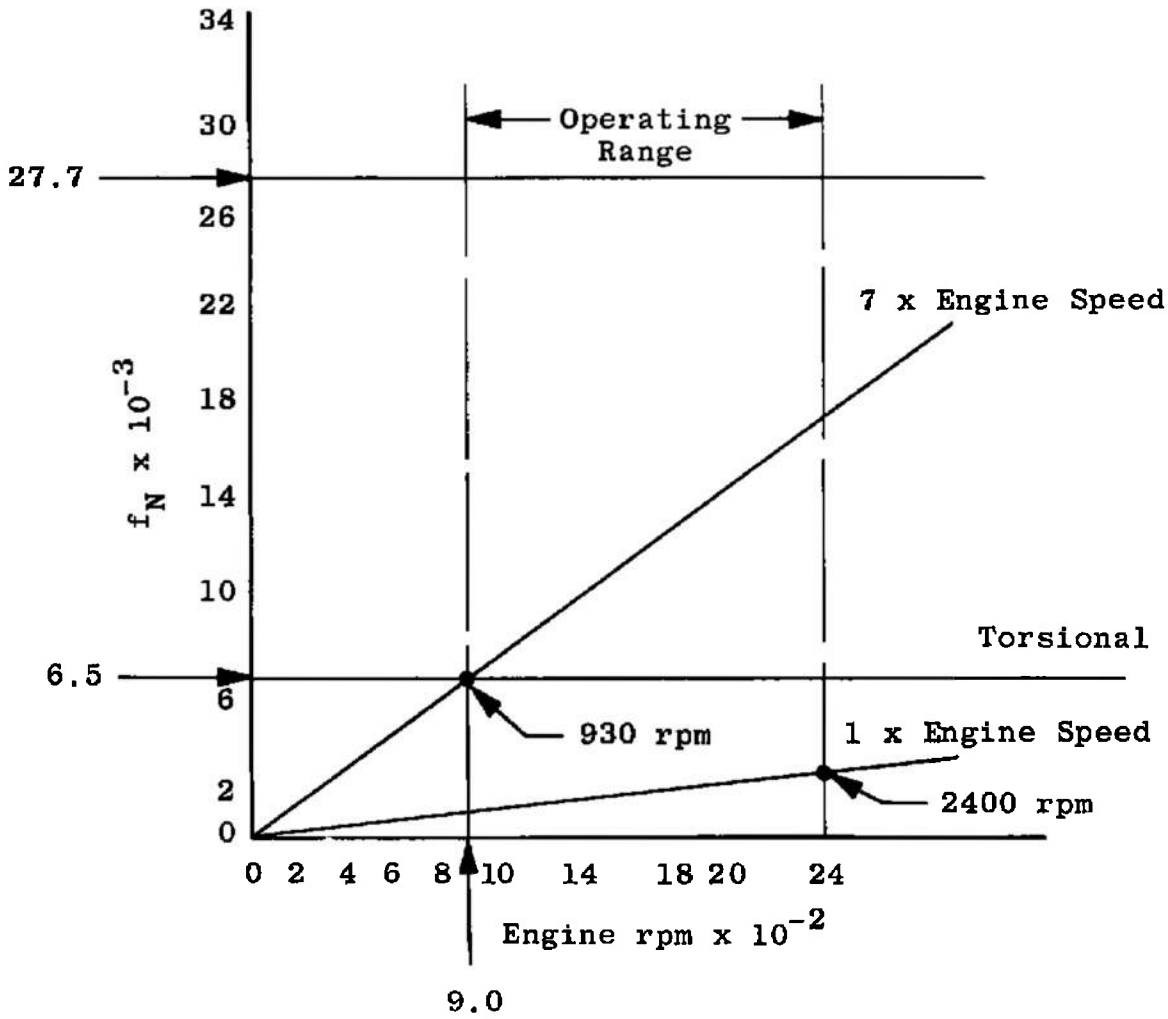

REFERENCE SHEET

Reference Dwgs:

1. ARO, Inc. Dwg. No. S 30A-0174
   Dwg. No. S 30A-0343

2. Koppers Co., Inc. Dwg. No. CC 24462

3. Allison Division Dwg. No. 6823505
   General Motors Corp. Dwg. No. AL 14267

4. Western Gear Corp. Dwg. No. D-303-357

Reference Correspondence:

5. Allison Division Reference No. 7339-SP-542
Indianapolis 6, Ind.

Reference Calculation:

6. ARO, Inc. Report No. CEB-016-03
Engineering Support Facility
Central Engineering Branch

APPENDIX II
CRITICAL SPEED ANALYSIS OF THE SUPERSONIC COMPRESSOR ROTOR

INTRODUCTION

This calculation contains a critical speed analysis of the supersonic compressor integral shaft and rotor.

CONCLUSIONS

The critical speed of the shaft and rotor is approximately 34,100 rpm. This is considerably above the operating speed of 16,680 rpm.

The maximum bearing load on the front bearing is 540 lb.

RECOMMENDATIONS

The following recommendations are made from the results of this investigation:

1. Make the diameter of the shaft 2.8 in. (This is maximum from bearing manufacturing restrictions.)

2. Keep the clearance between the shaft and the thrust bearings (pair) within the 0.0006 in. maximum fit clearance dimension specified by the ESF Mechanical Design.

3. Keep the unbalance of the rotor within the 3 gm-in. maximum unbalance as specified by the ESF Mechanical Design.

DISCUSSION

The analysis made was based on conservative assumptions. With the critical speeds calculated being considerably higher than the operating speeds, the concern for stiffness at the bearing locations was somewhat relieved. The bearing and shaft housing is actually massive and will add stiffness to the assembly. Since the critical speeds were calculated using the flexibility matrix method for the assumed two-degree-of-freedom system, the added stiffness would increase the critical speeds.

The thrust bearings actually tend to fix the shaft at their position. However, since information on the alignment

and tolerances was not known at the time of this computation, it was assumed that the analytical model was pinned at the bearing location.

The maximum bearing loads were calculated for the operating speed only.

ANALYSIS

This appendix presents a supersonic compressor critical speed analysis. Also included is a calculation of the maximum lateral bearing loading to be expected during operation within the design speed range.

The calculations showed no resonant critical or whirl speeds in or near the operating range. A low frequency reverse whirl was encountered below the normal operating range but should be of no significance.

The critical compressor speeds ranged from 5188 cpm at zero rotational speed to 34,200 cpm at 34,200 rpm, which is well above the normal operating range.

The bearing loads calculated were quite moderate. At 100 percent rpm the total forward bearing load was 540 lb. Approximately 50 percent of this load was due to the deadweight of the rotor assembly and the rest to the maximum allowable out-of-balance of 3 gm-in.

The following analysis was made to determine the presence of any critical rotational speeds of a supersonic test compressor system within its normal operational speed range. Under such a condition a set of critical frequencies was not found, but merely a lower limit of the set. Under this premise, considerable simplifications were possible. Thus the results should be construed only as qualitative.

Also included in the analysis is an estimate of the lateral bearing loads based on the same conservative assumptions as the critical speed analysis.

DESCRIPTION OF SYSTEM

The following dimensions and properties were obtained from Ref. 1:

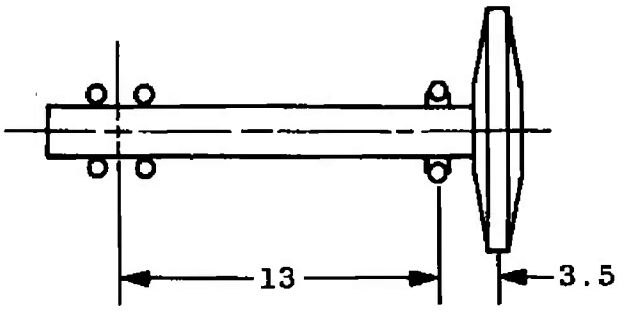

$I_{D\text{-}disc} \approx 30$ snails-in.^{2}

$W_{shaft} = 26$ lb

$W_{disc} = 232$ lb

$EI_{shaft} = 81.6 \times 10^6$ lb-in.^{2}

Fig. II-1

ASSUMPTIONS

The weight of the shaft is only a small portion of the weight of the disc. Therefore, the majority of the inertia loads on the system will be attributable to the large mass. To neglect completely the small mass would be unconservative. The small mass will be assumed concentrated at the center of the beam.

The thrust bearings are mounted rigidly to a solid frame. The bearings will resist shaft lateral rotations to a large degree. However, because of the lack of information concerning their stiffness, the joint will be assumed pinned, i.e., infinite lateral stiffness and zero rotational stiffness. The bearing clearances will be effectively zero with a thrust load on the shaft.

The large disc bearing will be assumed pinned as in the thrust bearing idealization. This assumption is not as safe though. Again, because of the massiveness and stiffness of the bearing housing, the stiffness of the large bearing and close tolerances there-of, the idealization is felt to have small errors well compensated for elsewhere.

Figure 2 represents the resulting two-degree-of-freedom system.

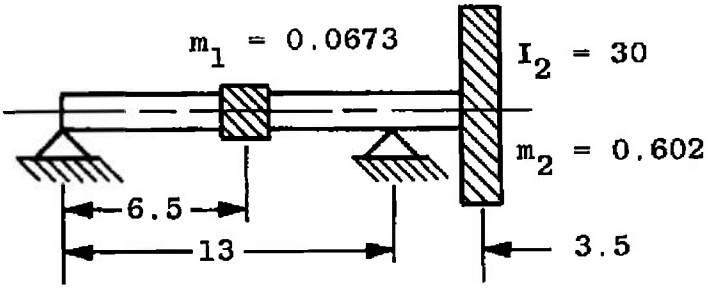

Fig. II-2

CALCULATIONS

Effect of Neglecting 26-lb Mass

The first calculations will be made to determine the effect of neglecting the 26-lb mass. This will be done to simplify the calculation concerning the inclusion of the gyroscopic stiffening effect.

First, the flexibility matrix for the simplified system of Fig. II-2 is calculated:

a_{11} = Deflection of m_1 attributable to a 1-lb load at m_1

$$a_{11} = \frac{L^3}{48EI} = \frac{13^3}{48EI} = \frac{45.77}{EI} \qquad \text{(Ref. 2)}$$

a_{21} = Deflection of m_2 attributable to a 1-lb load at m_1

$$a_{21} = -\theta_B L_{M_2} = \frac{-L^2}{16EI}(L_{m_2}) = \frac{-13^2 \times 3.5}{16EI} \qquad \text{(Ref. 2)}$$

$$a_{21} = \frac{-36.97}{EI}$$

a_{22} = Deflection of m_2 attributable to a 1-lb load at m_2

a_{22} = Deflection at 2 attributable to cantilever bending plus deflection attributable to slope at bearing support.

$$a_{22} = \frac{(2.5)^3}{3EI} + \frac{2.5^2}{2EI} + \frac{3.5 \times 13 \times 2.5}{3EI}$$

$$+ \frac{20.79}{EI} \qquad \text{(Ref. 2)}$$

where 2.5 in. is the effective length of the 3.5-in. section undergoing flexure.

$$a_{22} = \frac{5.208}{EI} + \frac{3.125}{EI} + \frac{37.917}{EI} + \frac{20.79}{EI} = \frac{67.0423}{EI}$$

a_{12} = Deflection of m_1 attributable to a 1-lb load at m_2

Because of Maxwell's reciprocity theorem,

$$a_{12} = a_{21} = \frac{-36.97}{EI}$$

Hence, the flexibility matrix may be written

$$[a] = \frac{1}{EI}\begin{bmatrix} 45.77 & -36.97 \\ -36.97 & 67.04 \end{bmatrix}$$

and the stiffness matrix

$$[K] = \begin{bmatrix} K_{11} & K_{12} \\ K_{21} & K_{22} \end{bmatrix} = [a]^{-1} = EI\begin{bmatrix} 45.77 & -36.97 \\ -36.97 & 67.04 \end{bmatrix}^{-1}$$

The inversion of [a] may then be accomplished as follows:

$$[\text{adj.}] = \begin{bmatrix} 67.04 & 36.97 \\ 36.97 & 45.77 \end{bmatrix}$$

$$[\text{det.}] = (67.04)(45.77) - (36.97)^2$$

$$(\text{det.}) = 1701.6$$

$$[\text{inv.}] = \frac{1}{(\text{det.})}[\text{adj.}] = \frac{EI}{(1701.6)}\begin{bmatrix} 67.04 & 36.97 \\ 36.97 & 45.77 \end{bmatrix}$$

$$\text{and, } [K] = 10^6\begin{bmatrix} 3.215 & 1.773 \\ 1.773 & 2.195 \end{bmatrix}$$

where $EI = 81.6 \times 10^6$

In stiffness matrix form, the differential equations of motion may be written

$$\begin{bmatrix} m_1 & 0 \\ 0 & M_2 \end{bmatrix}\begin{bmatrix} \ddot{x}_1 \\ \ddot{x}_2 \end{bmatrix} + \begin{bmatrix} K_{11} & K_{12} \\ K_{21} & K_{22} \end{bmatrix}\begin{bmatrix} x_1 \\ x_2 \end{bmatrix} = \begin{bmatrix} F_1(t) \\ F_2(t) \end{bmatrix} \tag{1}$$

By applying the solution $x_i = X_i e^{i(\omega t+\phi)}$ and setting the forcing functions equal to zero, this equation may be written

$$\begin{bmatrix} K_{11} - m_1\omega^2 & K_{12} \\ K_{12} & K_{22} - m_2\omega^2 \end{bmatrix} \begin{bmatrix} x_1 \\ x_2 \end{bmatrix} = \begin{bmatrix} 0 \\ 0 \end{bmatrix} \tag{2}$$

This equality will yield a nontrivial solution in $[x_i]$ only if the determinate vanishes. Thus,

$$(K_{11} - m_1\omega^2)(K_{22} - m_2\omega^2) = K_{12}^2$$

Expanding,

$$K_{11} K_{22} - K_{12}^2 - K_{11}m_2\omega^2 - K_{22}m_1\omega^2 + m_1m_2\omega^4 = 0$$

Factoring,

$$m_1m_2\omega^4 - (K_{11}m_2 + K_{22}m_1)\omega^2 + (K_{11}K_{22} - K_{12}^2) = 0$$

Solving for ω^2,

$$\omega^2 = \frac{(K_{11}m_2+K_{22}m_1) \pm \sqrt{(K_{11}m_2+K_{22}m_1)^2-4m_1m_2(K_{11}K_{22}-K_{12}^2)}}{2m_1m_2}$$

Substituting in this equation,

$$(K_{11}m_2 + K_{22}m_1) = (3.215)(0.602) \times 10^6 + (2.195)(0.0673) \times 10^6 = 2.083 \times 10^6$$

$$4m_1m_2(K_{11}K_{22} - K_{12}^2) = 4(0.602)(0.0673)\,[3.215(2.195) - (1.773)^2] \times 10^{12} = 0.634 \times 10^{12}$$

$$2m_1m_2 = 2(0.602)(0.0673) = 0.08103$$

$$\omega^2 = \frac{(2.083 \pm \sqrt{(2.083)^2 - 0.634})}{0.08103} \times 10^6$$

$$\omega^2 = \frac{(2.083 \pm \sqrt{3.7049})}{0.08103} \times 10^6$$

$$\omega^2 = \frac{(2.083 \pm 1.9248)}{0.08103} \times 10^6$$

$$\omega_1 = 1397 \text{ rad/sec} \longleftarrow$$

$$\omega_2 = 7054 \text{ rad/sec}$$

Next, when $m_1 = 0$, Eq. (2) reduces to

$$K_{22} - m_2\omega^2 = 0$$

$$\text{or, } \omega_N = \sqrt{\frac{K_{22}}{m_2}} = \sqrt{\frac{2.195 \times 10^6}{0.602}} = 1909 \text{ rad/sec}$$

Thus, m_1, though small compared to m_2, must be considered in the more extensive analysis.

Effect of Gyroscopic Stiffening

The following analysis includes the effect of gyroscopic stiffening. To keep the analysis from getting out of hand, namely increasing the number of degrees of freedom from two to three, an approximation will be made which is safe for systems with wide spread first and second modes. This approximation is the increasing of m_2 to some $m_{2_{eff}}$ such that the structural properties remain the same but the new single-degree-of-freedom system has the same ω_N.

$$\text{Thus,} \qquad \omega_N = \sqrt{\frac{K_{22}}{m_{2_{eff}}}}$$

$$\text{or} \qquad m_{2_{eff}} = \frac{K_{22}}{\omega_N^2} = \frac{2.195 \times 10^6}{1.952 \times 10^6}$$

$$m_{2_{eff}} = 1.124$$

The gyroscopic stiffening may be included as given in Ref. 3. The new set of influence coefficients may be calculated as follows for the modified Fig. II-3:

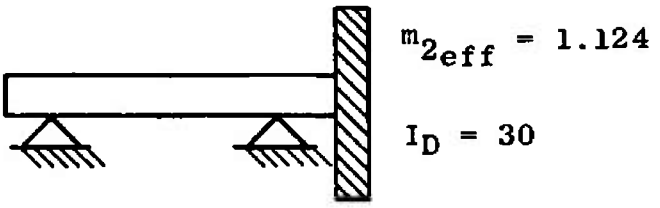

Fig. II-3

b_{11} = Deflection of m_2 attributable to a 1-lb load at m_2

$$b_{11} = \frac{67.04}{EI}$$

b_{21} = Rotation of I_D attributable to a 1-lb load at m_2

b_{21} = Slope at bearing plus slope caused by 3.5 in. cantilever

$$b_{21} = \frac{(1)(2.5)^2}{2EI} + \frac{(1)^2(2.5)}{EI} + \frac{3.5(13)}{3EI}$$

$$b_{21} = \frac{20.79}{EI}$$

b_{22} = Rotation of I_D attributable to a 1-in.-lb torque at I_D

$$b_{22} = \frac{(1)(13)}{3EI} + \frac{(1)(2.5)}{EI} = \frac{6.833}{EI}$$

b_{12} = Deflection of m_2 attributable to a 1-in.-lb torque at I_D

$$b_{12} = b_{21} = \frac{20.79}{EI}$$

Hence, the flexibility matrix is

$$[b] = \frac{1}{EI}\begin{bmatrix} 67.04 & 20.79 \\ 20.79 & 6.833 \end{bmatrix}$$

Let the beam loading be $m_2\omega^2 x_2$ and $-I_D\omega^2\phi$ for the inertia and gyroscopic loads, respectively. Then,

$$\begin{bmatrix} x_2 \\ \phi \end{bmatrix} = \frac{1}{EI} \begin{bmatrix} 67.04 & 20.79 \\ 20.79 & 6.833 \end{bmatrix} \begin{bmatrix} m_2\omega^2 x_2 \\ -I_D\omega^2\phi \end{bmatrix}$$

By subtracting the left side of this equation from both sides and rearranging,

$$\begin{bmatrix} 0 \\ 0 \end{bmatrix} = \begin{bmatrix} \dfrac{(67.04m_2\omega^2-1)}{EI} & \dfrac{-20.79I_D\omega^2}{EI} \\ \dfrac{20.79m_2\omega^2}{EI} & \dfrac{(-6.833I_D\omega^2-1)}{EI} \end{bmatrix} \begin{bmatrix} x_2 \\ \phi \end{bmatrix}$$

Substituting $EI = 81.6 \times 10^6$, $m_2 = 1.124$, and $I_D = 30$,

$$\begin{bmatrix} 0 \\ 0 \end{bmatrix} = \begin{bmatrix} (0.9234 \times 10^{-6}\omega^2-1) & -7.643 \times 10^{-6}\omega^2 \\ 0.2864 \times 10^{-6}\omega^2 & -(2.512 \times 10^{-6}\omega^2+1) \end{bmatrix} \begin{bmatrix} x_2 \\ \phi \end{bmatrix}$$

For a nontrivial solution to exist, the determinant of this equation must vanish. Thus,

$$-(0.9234 \times 10^{-6}\omega^2-1)(2.512 \times 10^{-6}\omega^2+1)$$

$$+ (0.2864 \times 10^{-6}\omega^2)\ (7.643 \times 10^{-6}\omega^2) = 0$$

Expanding

$$- [(0.9234)(2.512)\omega^4 \times 10^{-12} + 0.9234 \times 10^{-6}\omega^2$$

$$- 2.512 \times 10^{-6}\omega^2-1] + [(0.2864)(7.643)\omega^4 \times 10^{-12}]$$

$$= 0$$

$$+ [2.3196 \times 10^{-12}\omega^4 -1.5886 \times 10^{-6}\omega^2-1]$$

$$- 2.189 \times 10^{-12}\omega^4 = 0$$

$$0.1306 \times 10^{-12}\omega^4 - 1.5886 \times 10^{-6}\omega^2-1 = 0$$

Substituting in the quadratic equation,

$$\omega^2 = \frac{1.5886 \times 10^{-6} \pm \sqrt{(1.5886)^2 + 4(0.1306)} \times 10^{-6}}{2(0.1306) \times 10^{-12}}$$

$$\omega^2 = \frac{1.5886 \times 10^{-6} \pm \sqrt{3.046} \times 10^{-6}}{0.2612 \times 10^{-12}}$$

$$\omega^2 = \frac{1.5886 \pm 1.745}{0.2612} \times 10^6$$

For the only real root,

$$\omega_N = \sqrt{12.76} \times 10^3$$

$$\omega_N = 3572 \text{ rad/sec}$$

Whirl Critical Frequencies

To establish the validity of the 3572-rad/sec critical frequency, a check will be made on the possibility of whirl critical frequencies in the operating range. This is felt to be necessary because of the large off-diagonal flexibility matrix terms.

The following analysis was obtained from Ref. 3, page 262.

$$\omega^4(-m\alpha_{11}\alpha_{22}I_D + m\alpha_{13}{}^2 I_D) + \omega^3(m\alpha_{11}\alpha_{22}I_D 2\Omega - m\alpha_{12}{}^2 I_D 2\Omega)$$

$$+ \omega^2(\alpha_{22}I_D + m\alpha_{11}) + \omega(-\alpha_{22}I_D 2\Omega) - 1 = 0$$

where

Ω = shaft rotational speed

ω = whirl frequency

α_{ij} = influence coefficients

I_D = mass moment of inertia about a diameter

m = mass of disk.

This equation is more simply written as

$$F^4 - 2SF^3 + \frac{D+1}{D(E-1)}F^2 - \frac{2\ S}{E-1}F - \frac{1}{D(E-1)} = 0$$

where

$$F = \omega\sqrt{\alpha_{11}m} = \omega\sqrt{0.8216 \times 1.124} \times 10^{-3}$$

$$= \omega(0.961) \times 10^{-3}$$

$$D = \frac{I_D\alpha_{22}}{m\alpha_{11}} = \frac{30 \times 0.0837}{1.124(0.8216)} = 2.719$$

$$E = \frac{\alpha_{12}^{\ 2}}{\alpha_{11}\alpha_{22}} = \frac{(0.2548)^2}{(0.8216)(0.0837)} = 0.9441$$

$$S = \Omega\sqrt{\alpha_{11}m} = \Omega\sqrt{0.9235} \times 10^{-3} = \Omega(0.961) \times 10^{-3}$$

Substituting,

$$0.8529 \times 10^{-12}\omega^4 - 1.7057 \times \omega^3\Omega \times 10^{-12} - 22.575\omega^2 \times 10^{-6}$$

$$+ 33.011 \times 10^{-6}\omega\Omega + 6.5733 = 0$$

Normalizing,

$$\omega^4 - 2\Omega\omega^3 \times 10^{-12} - 26.468\omega^2 \times 10^{-6} + 38.704\ \omega\Omega \times 10^{-6}$$

$$+ 7.7069 = 0$$

Whirl divergence occurs when the rotational speed, Ω, corresponds to the whirl speed, ω. Forward whirl divergence occurs when $\omega = \Omega = \omega_N$, or

$$\omega_N^{\ 4} - 2\omega_N\omega_N^{\ 3} \times 10^{-12} - 26.464\ \omega_N^{\ 2} \times 10^{-6} + 38.704\omega_N^{\ 2}$$

$$\times 10^{-6} + 7.7069 = 0.$$

Combining,

$$-\omega_N^4 + 12.24\ \omega_N^2 \times 10^6 + 7.7069 \times 10^{12} = 0$$

Normalizing,

$$\omega_N^4 - 12.24\ \omega_N^2 \times 10^6 - 7.7069 \times 10^{12} = 0$$

which has roots

$$\omega_N^2 = \left[\frac{12.24 \pm \sqrt{(12.24)^2 + 30.828}}{2}\right] 10^3$$

$$= \frac{12.24 \pm 13.43}{2} \times 10^3$$

But, the only real root is $[(12.24 + 13.43)/2]^{1/2} \times 10^3$ or the whirl divergence speed is

$$\omega_{N_W} = 3582 \text{ rad/sec}$$

For negative whirl divergence, $\Omega = -\omega$ and

$$\omega_N^4 + 2\omega_N^4 \times 10^{-12} - 26.468\omega_N^2 \times 10^{-6} - 38.704\omega_N^2 \times 10^{-6}$$

$$+ 7.7069 = 0$$

$$3\omega_N^4 - 65.172\omega_N^2 \times 10^6 + 7.7069 \times 10^{12} = 0$$

Normalizing,

$$\omega_N^4 - 21.724\omega_N^2 \times 10^6 + 2.569 \times 10^{12} = 0$$

which has the roots

$$\omega_N^2 = \frac{21.724 \pm \sqrt{(21.724)^2 - 4(2.569)}}{2}$$

$$\omega_N^2 = \left(\frac{21.724 \pm \sqrt{461.65}}{2}\right) 10^6$$

The negative whirl divergence speeds are then

$$\omega_{N_{W_1}} = -490 \text{ rad/sec}$$

and

$$\omega_{N_{W_2}} = -4650 \text{ rad/sec}$$

It is felt that no trouble should be encountered with the 490-rad/sec negative whirl speed since it is well below the operating range. Also, the energy fed into negative whirl modes is of questionable origin and generally does not appear.

The last and possibly the most useful critical frequency to be calculated is the zero rpm natural frequency. It will serve as a check on the assumptions made of bearing stiffnesses discussed earlier.

This frequency is calculated by setting the value of Ω in the whirl equation to zero.

Thus,

$$\omega^4 - 26.468\omega^2 \times 10^{-6} + 7.7069 = 0$$

which has roots calculated by

$$\omega^2 = \frac{26.468 \pm \sqrt{(26.468)^2 - 4(7.7069)}}{2} \times 10^6$$

$$\omega^2 = 1/2\ (26.468 \pm \sqrt{-669.73} \times 10^6 = 0.295 \times 10^6$$

Finally, $\omega_{N_{\Omega=0}} = 543$ rad/sec

By the use of an electrodynamic shaker, this mode may be excited during the rotor assembly, before initial run-up, thus completing the vibration check-out.

SUMMARY CHART

Static critical = 543 rad/sec = 86.7 cps = 5,188 rpm

Negative whirl = -490 rad/sec = -78 cps = -4,680 rpm

Forward whirl = 3582 rad/sec = 570 cps = 34,200 rpm

First critical = 3575 rad/sec = 569 cps = 34,100 rpm

BEARING LOAD CALCULATIONS

Bearing loads will be calculated for the simplified system of Fig. II-3. The flexibility matrix is

$$[b] = \frac{1}{EI}\begin{bmatrix} 67.04 & 20.79 \\ 20.79 & 6.833 \end{bmatrix}$$

Since $EI = 81.6 \times 10^6$,

$$[b] = 10^6 \begin{bmatrix} 0.822 & 0.255 \\ 0.255 & 0.0837 \end{bmatrix}$$

The stiffness matrix may be determined by inversion as follows:

$$|D| = 10^{12}\ (0.068801 - 0.065025) = 0.003776 \times 10^{12}$$

$$[K] = \frac{10^6}{0.003776}\begin{bmatrix} 0.0837 & -0.255 \\ -0.255 & 0.822 \end{bmatrix}$$

$$[K] = 10^6 \begin{bmatrix} 22.13 & -63.4 \\ -63.4 & 217.5 \end{bmatrix}$$

Since the compressor acts below the critical speed range, the maximum bearing loading will occur at 16,680 rpm or 1746.7 rad/sec.

The dynamic stiffness matrix becomes

$$[K_{dyn}] = \begin{bmatrix} K_{11}-M_1W^2 & K_{12} \\ K_{12} & K_{22}+I_DW^2 \end{bmatrix}$$

$$\text{or } [K_{dyn}] = \begin{bmatrix} 22.13 - (1.124 \times 3.051) & -63.4 \\ -63.4 & 217.5+30(3.051) \end{bmatrix} \times 10^6$$

$$[K_{dyn}] = 10^6 \begin{bmatrix} 18.70 & -63.4 \\ -63.4 & 309.03 \end{bmatrix}$$

and the dynamic flexibility matrix,

$$[F_{dyn}] = [K_{dyn}]^{-1}$$

$$|D| = (18.70)(309.03) - (63.4)^2 = 1760 \times 10^{12}$$

$$[F_{dyn}] = \frac{10^{-6}}{1760} \begin{bmatrix} 309.03 & 63.4 \\ 63.4 & 18.70 \end{bmatrix}$$

$$[F_{dyn}] = 10^{-6} \begin{bmatrix} 0.1752 & 0.036 \\ 0.036 & 0.01061 \end{bmatrix}$$

The application of a dynamic load may be accomplished as follows:

$$\{x\} = [F_{dyn}] \{P_{dyn}\}$$

$[P_{dyn}]$ is computed from the unbalance, 3 gm-in., to be

$$P_1 = \frac{3 \times 2.205 \times 10^{-3}}{386} \times 3.051 \times 10^6 = 52.28 \text{ lb}$$

$$T = 0$$

Thus, $x = (58.2)(0.1752)(10^{-6}) = 10.2 \times 10^{-6}$ in.

$$\phi = (0.036)(0.1752)(10^{-6}) = 0.00631 \times 10^{-6} \text{ rad}$$

which are the deflections under the dynamic load. The beam loading may now be computed by the use of the static stiffness matrix to be

$$\begin{bmatrix} P \\ T \end{bmatrix} = 10^6 \begin{bmatrix} 22.13 & -63.4 \\ -63.4 & 217.5 \end{bmatrix} \begin{bmatrix} 10.2 \times 10^{-6} \\ 0.00631 \times 10^{-6} \end{bmatrix}$$

$$P = 22.13 \times 10.2 - 63.4 \times 0.00631 = 222.5 \text{ lb}$$

$$T = -63.4 \times 10.2 + 217.5 + 0.00631 = -645 \text{ in.-lb}$$

The dynamic beam loading may be coupled with the static weight to compose the resultant bearing loads:

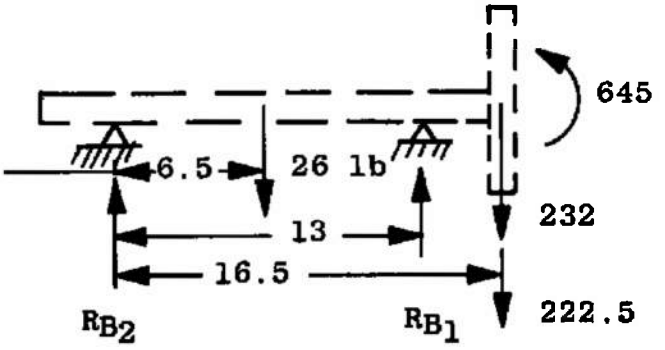

$$\Sigma m_{R_{B_2}} = 0 = (6.5)(26) + 16.5\ (232 + 222.5) - 645 - 13\ R_{B_1}$$

$$13\ R_{B_1} = 169 + 7{,}500 - 645$$

$$R_{B_1} = 540 \text{ lb (UP)}$$

$$R_{B_2} = (26 + 232 + 222.5) - 540$$

$$R_{B_2} = -59.5 \text{ lb (DOWN)}$$

REFERENCES

1. ARO Drawing ESF/CE SK-61 "Supersonic Compressor Test Rotor Bearing Layout."

2. Singer, F. L. "Strength of Materials." Harper, New York, N. Y. (Second Edition).

3. Den Hartog, J. P. "Mechanical Vibrations." McGraw-Hill, New York, N. Y. (Fourth Edition).

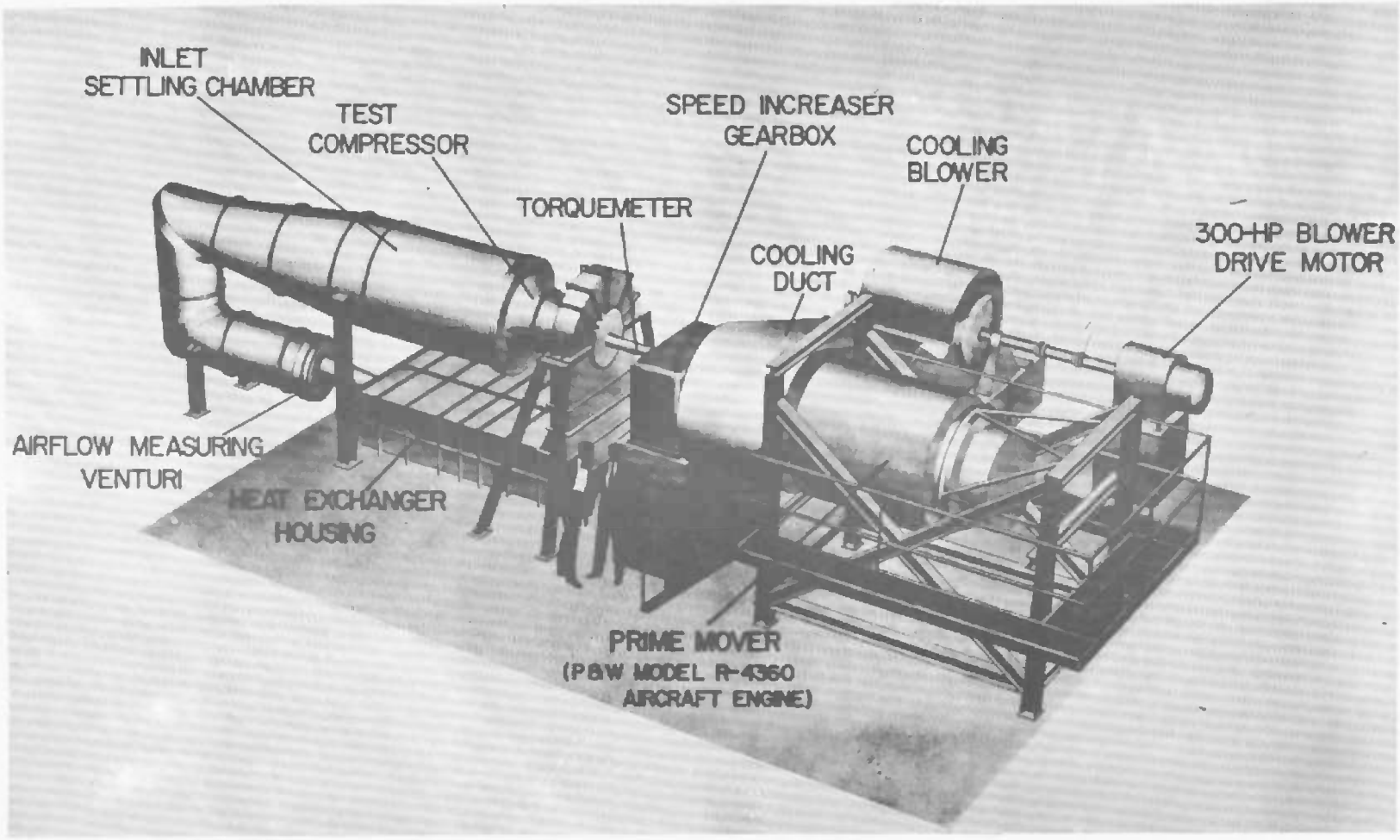

Fig. 1 Supersonic Compressor Test Rig

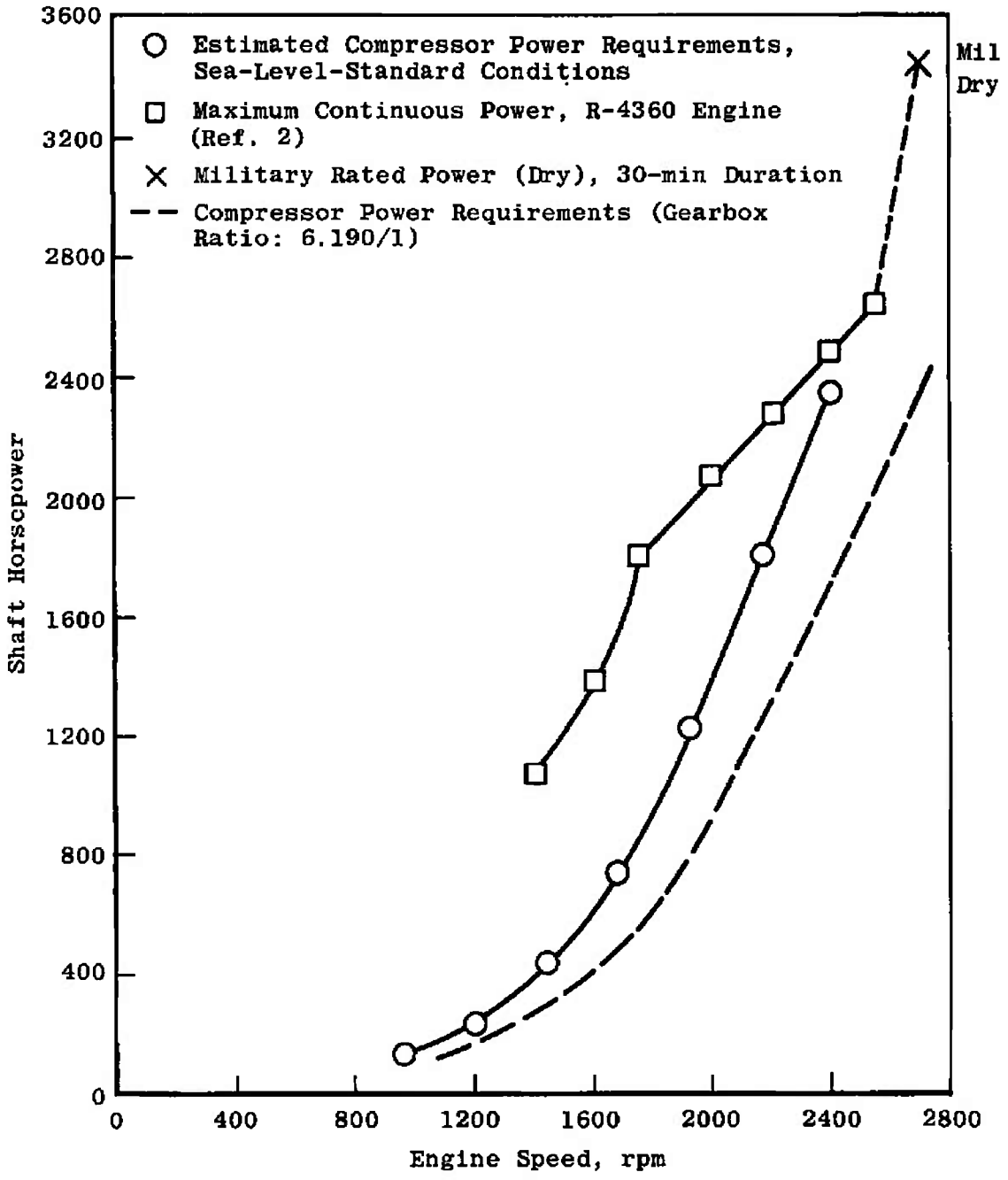

Fig. 2 Compressor Rig Power Requirements

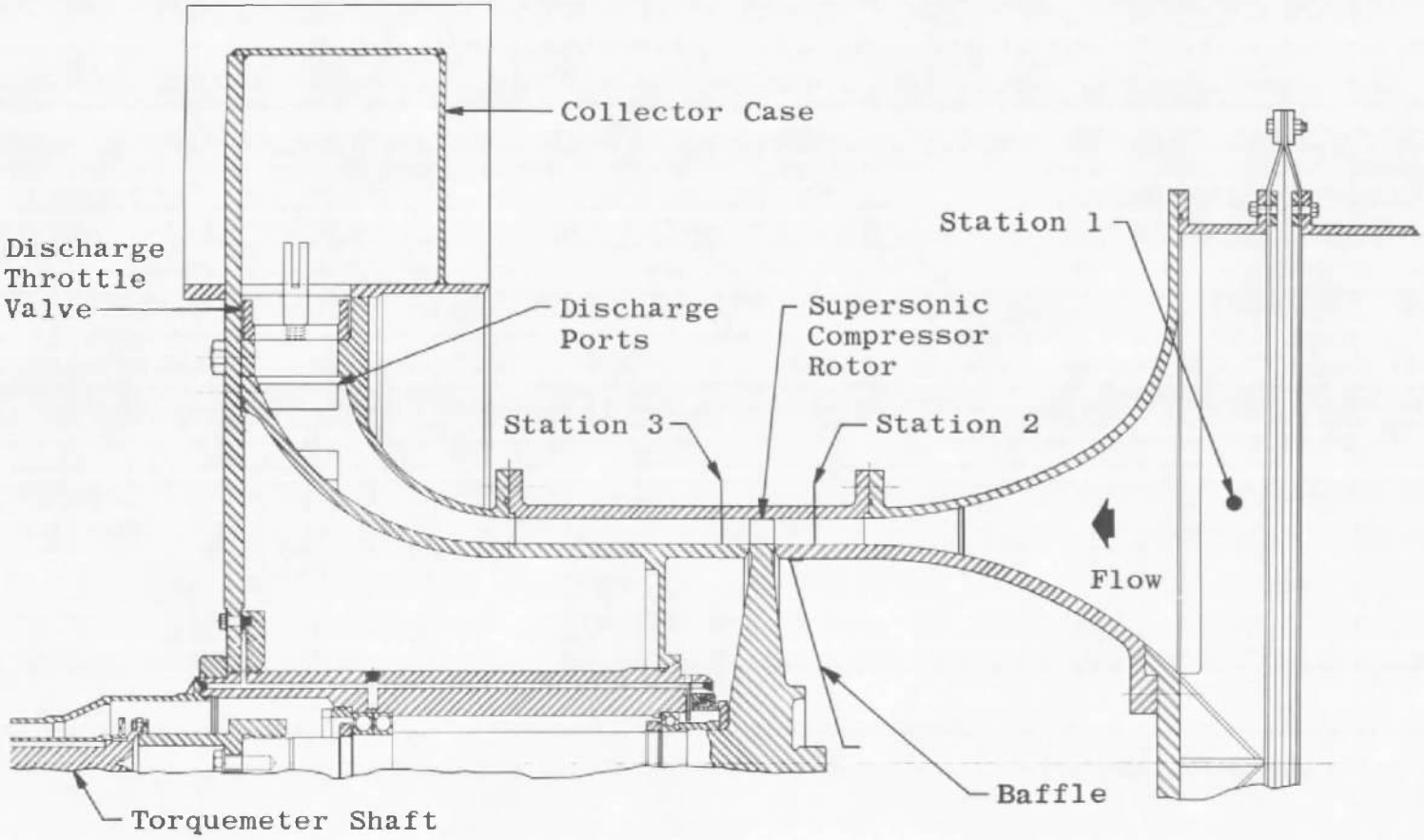

Fig. 3 Cross-Sectional View of Experimental Compressor

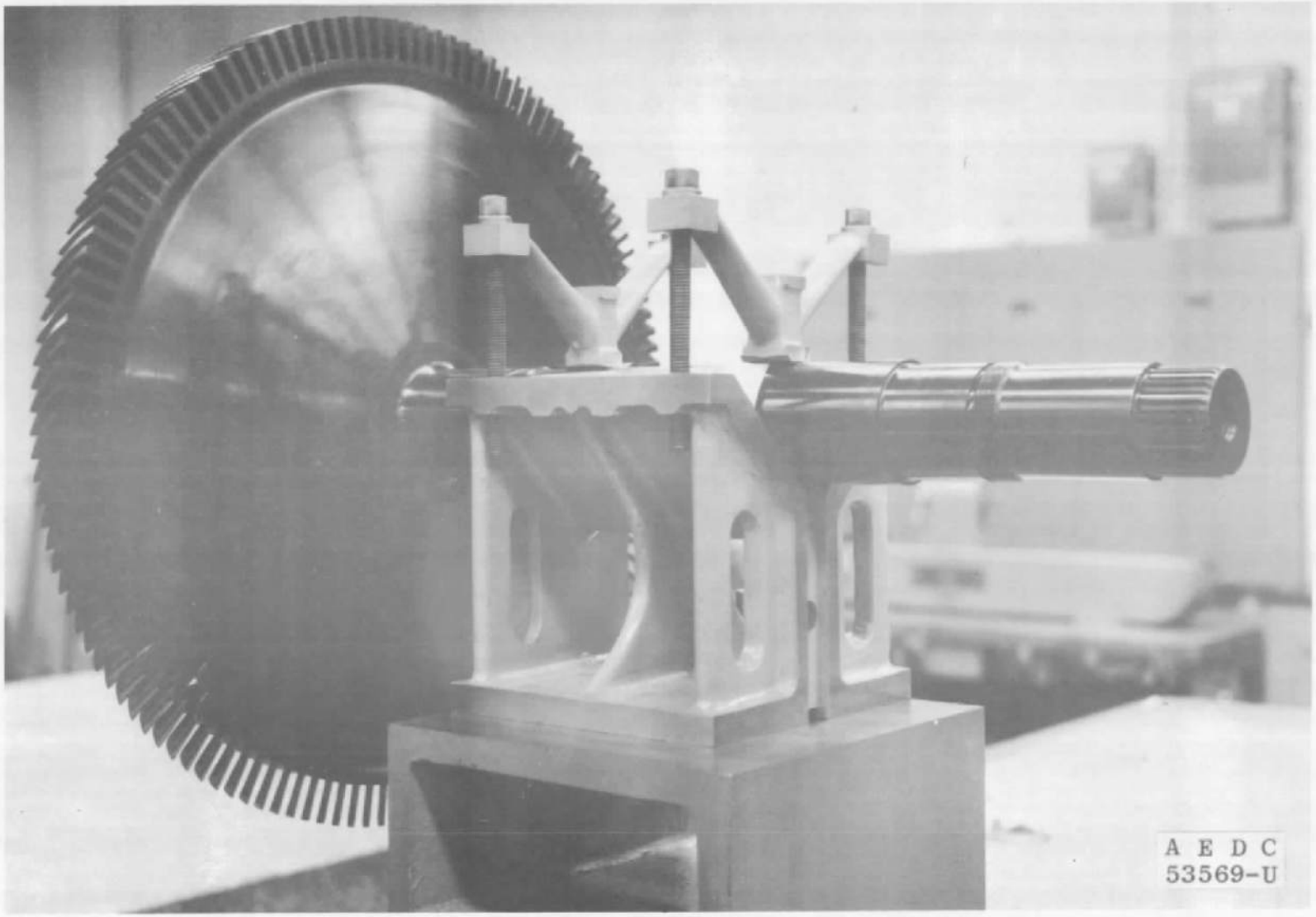

Fig. 4 Supersonic Compressor Rotor No. 1

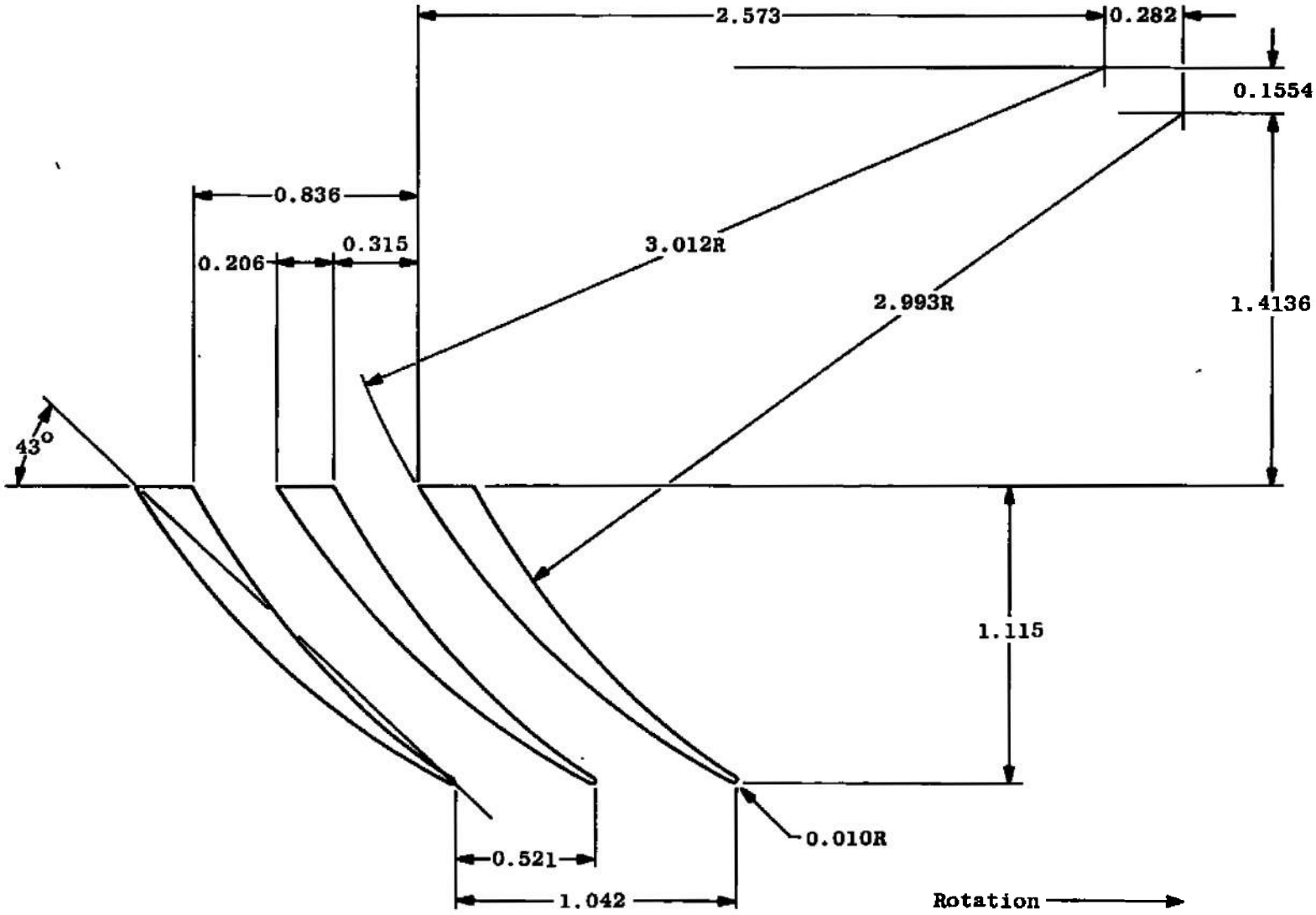

Fig. 5 Mean Radius Profile – Blunt Trailing Edge Blade No. 1

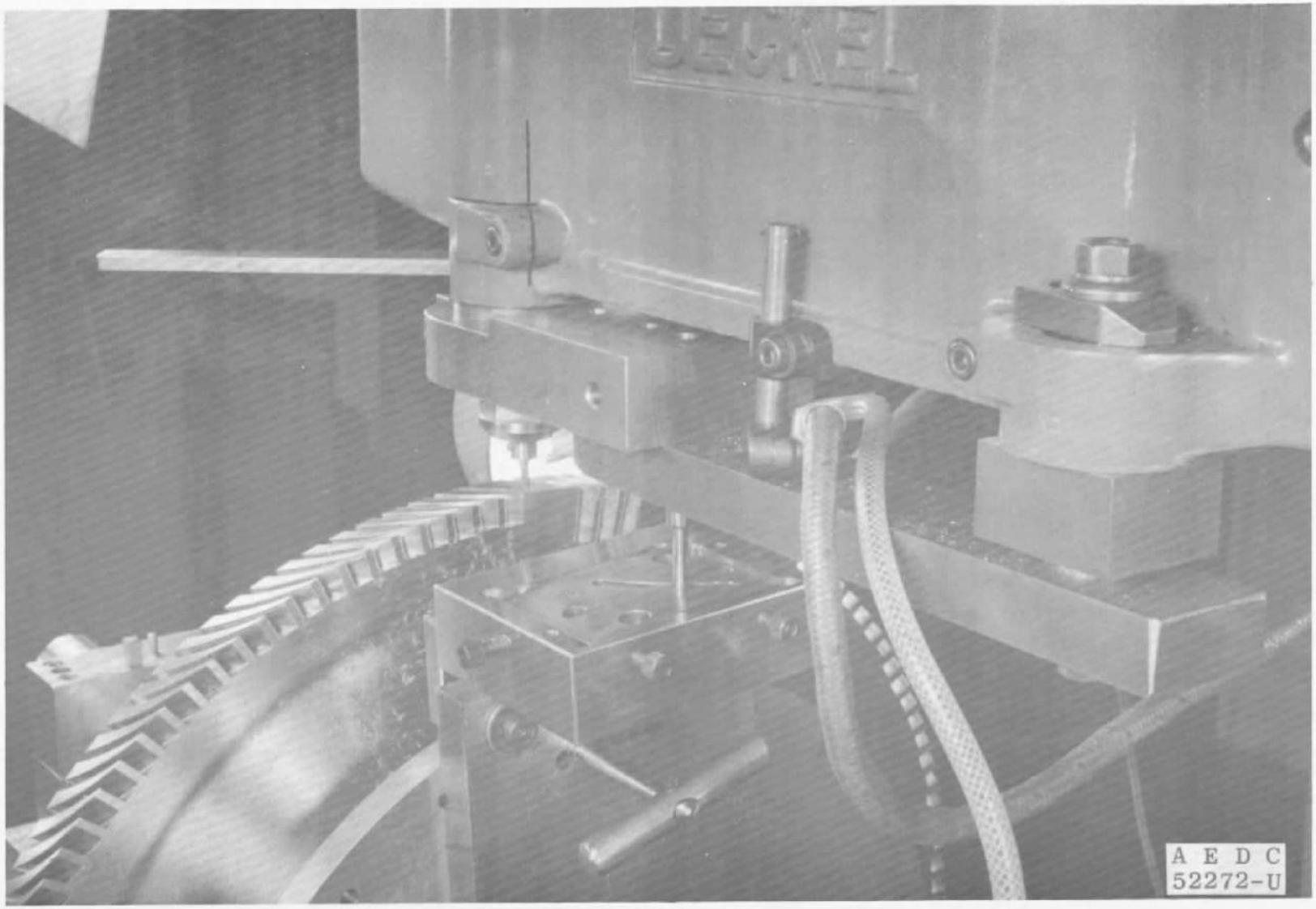

Fig. 6 Machine Setup for Generating the Blunt Trailing Edge Blading

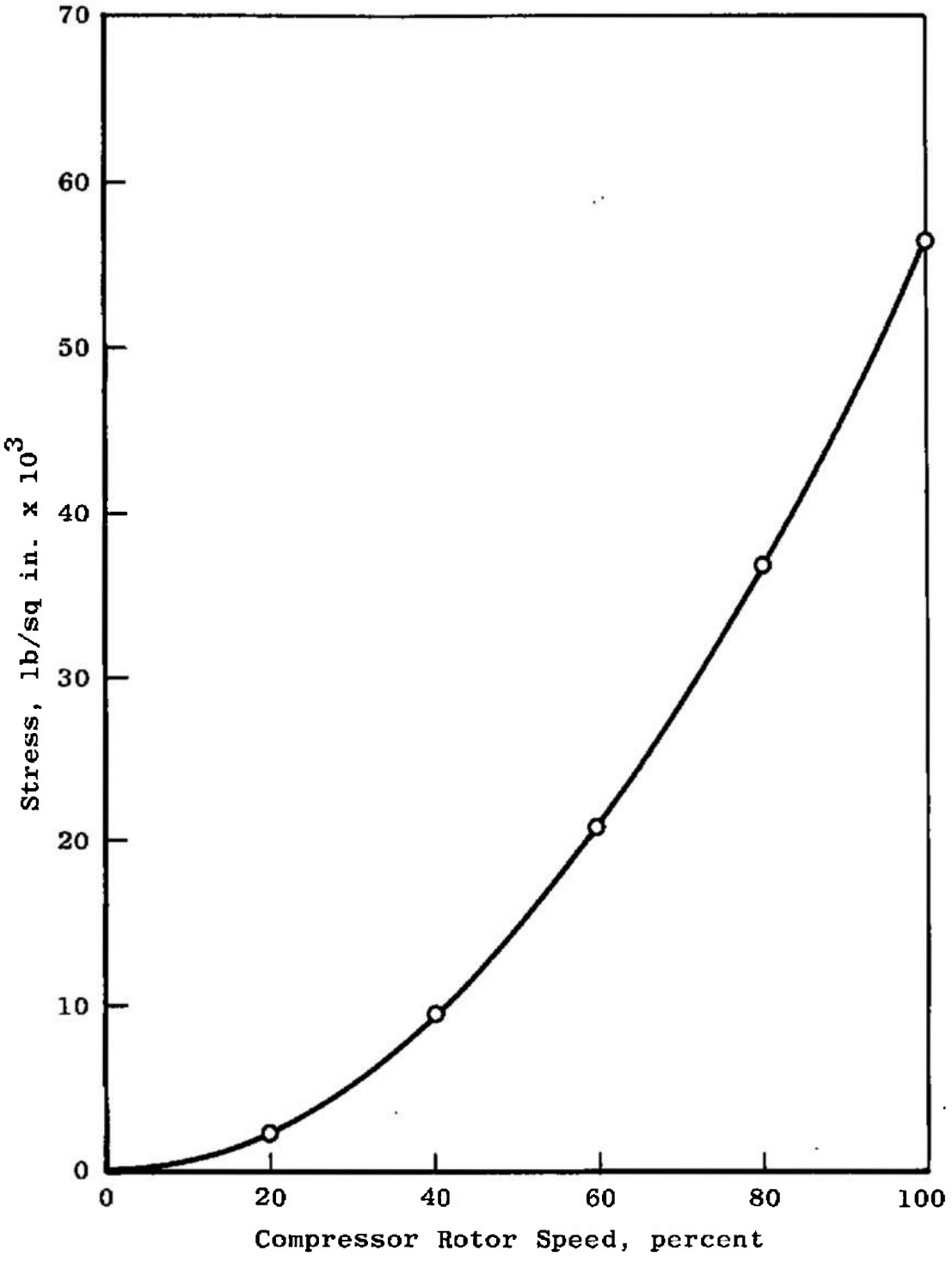

Fig. 7 Maximum Centrifugal Stress in the Supersonic Compressor Rotor

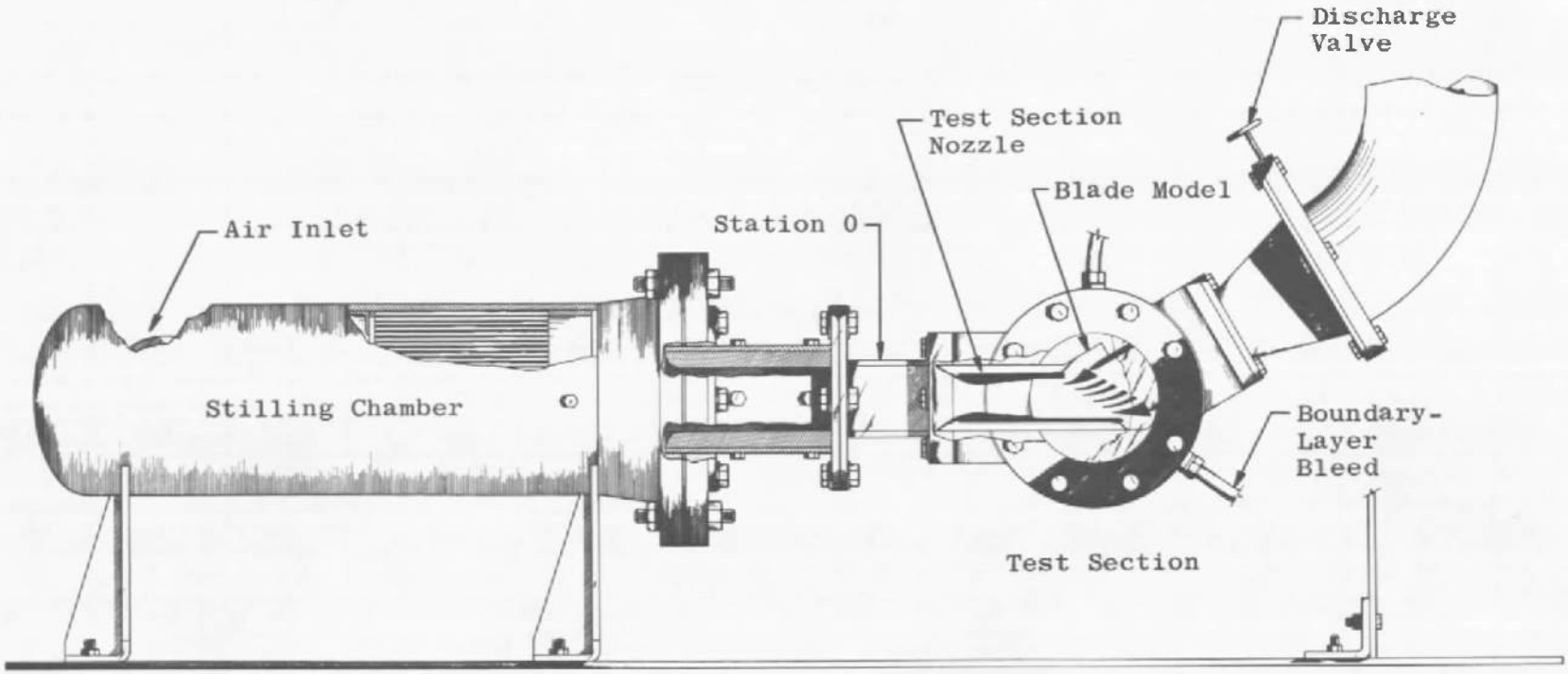

Fig. 8 Cascade Rig Supersonic Compressor Test

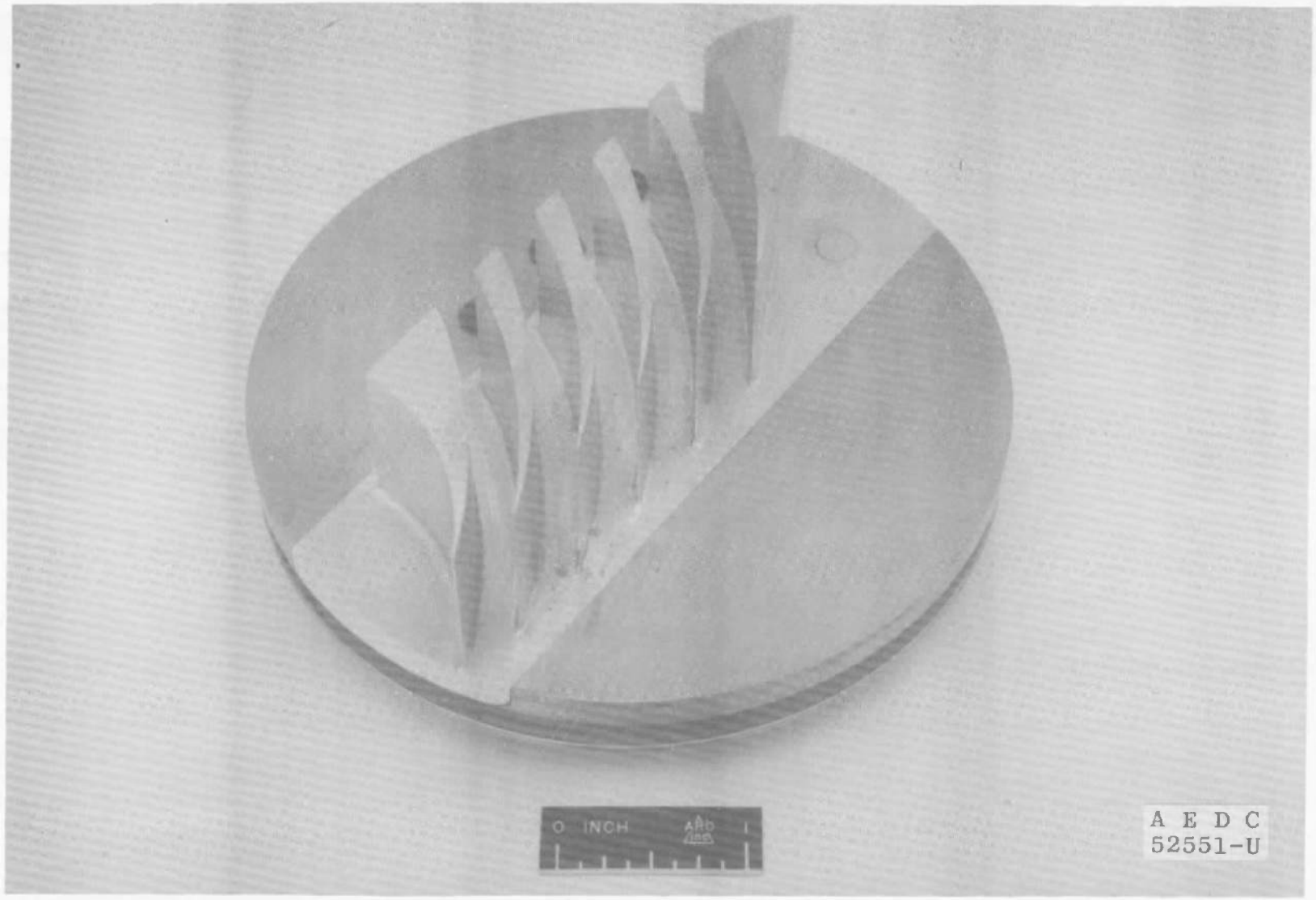

Fig. 9 Cascade Model No. 1 Circular-Arc Blades

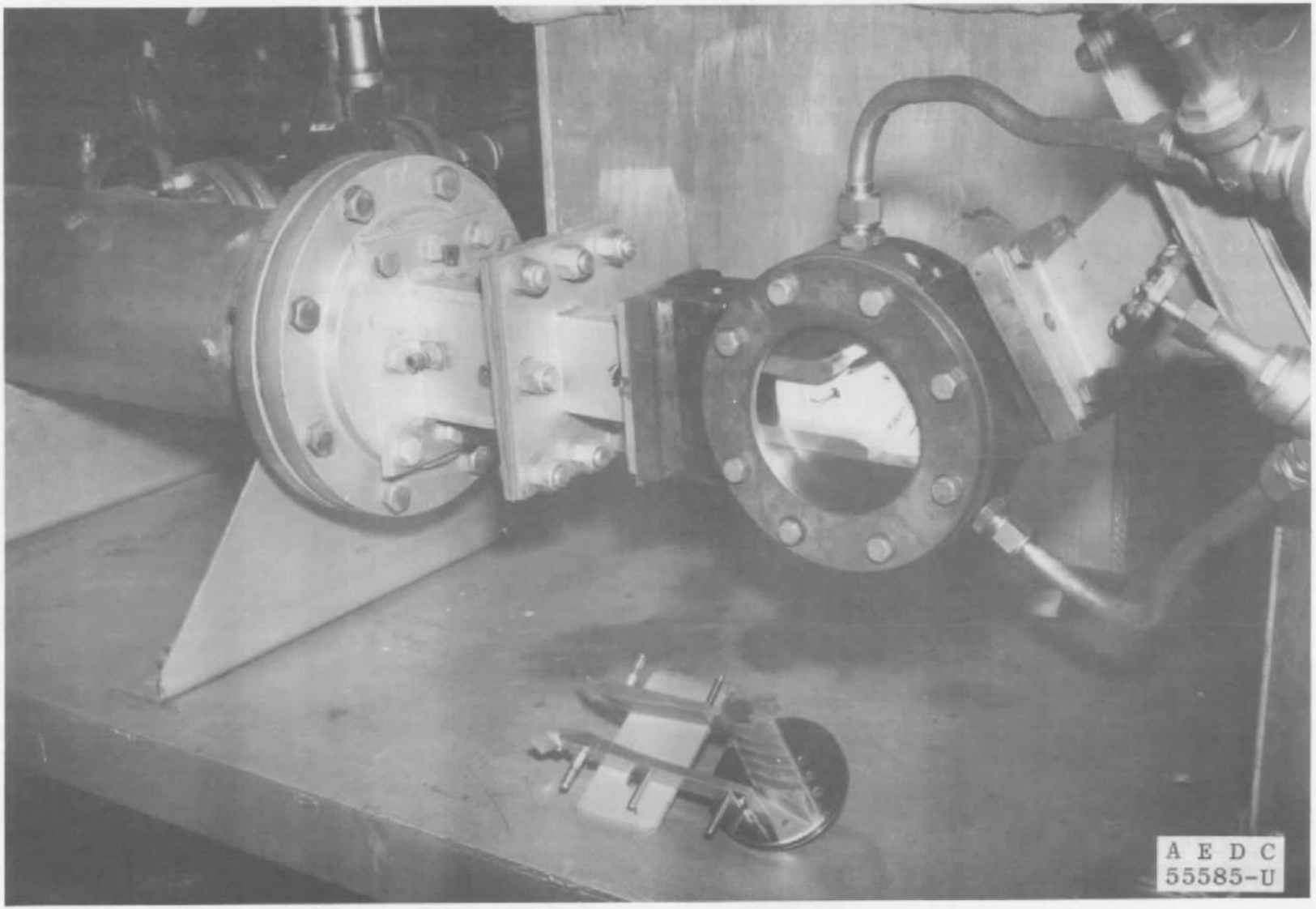

Fig. 10 Cascade Test Rig – Probe Calibration Configuration (Blade Test Setup Shown on Mounting Stand)

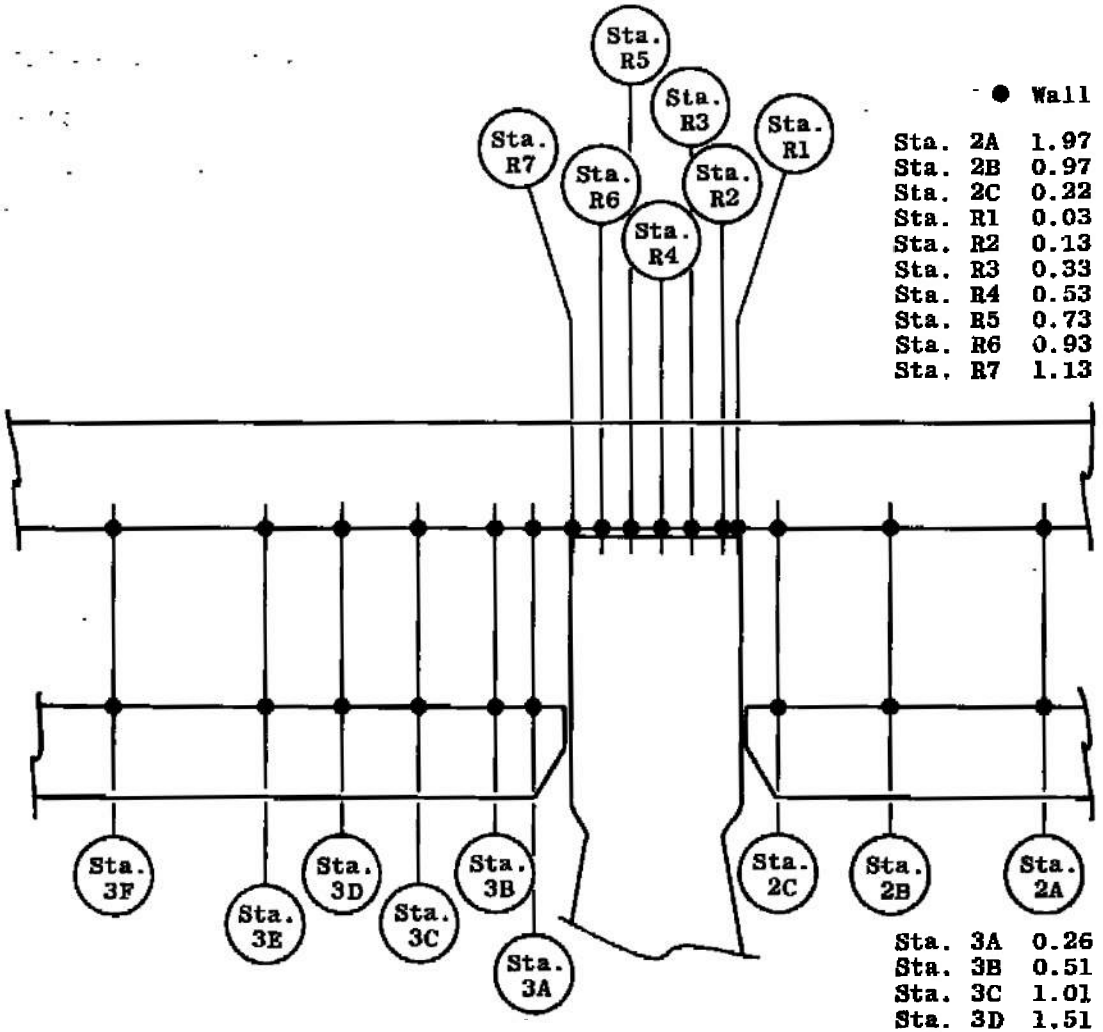

● Wall Static Pressure Taps

Sta. 2A	1.97 in.	Forward of	Leading	Edge
Sta. 2B	0.97 in.	"	"	"
Sta. 2C	0.22 in.	"	"	"
Sta. R1	0.03 in.	Behind	Leading	Edge
Sta. R2	0.13 in.	"	"	"
Sta. R3	0.33 in.	"	"	"
Sta. R4	0.53 in.	"	"	"
Sta. R5	0.73 in.	"	"	"
Sta. R6	0.93 in.	"	"	"
Sta. R7	1.13 in.	"	"	"

Sta. 3A	0.26 in.	Behind	Trailing	Edge
Sta. 3B	0.51 in.	"	"	"
Sta. 3C	1.01 in.	"	"	"
Sta. 3D	1.51 in.	"	"	"
Sta. 3E	2.01 in.	"	"	"
Sta. 3F	3.01 in.	"	"	"

a. Station Locations

Fig. 11 Details of Instrumentation Stations

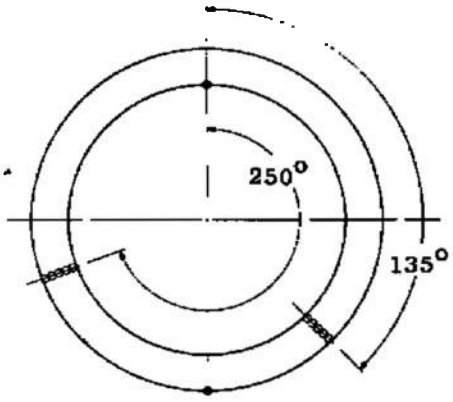

b. Station 2A

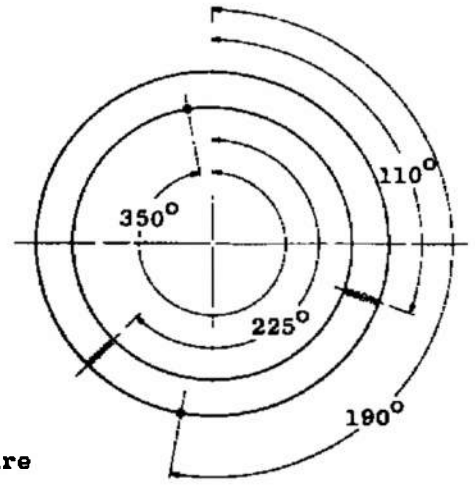

c. Station 2B

- ∘ Total Pressure
- • Static Pressure
- x Total Temperature
- Traverse
- Yaw Angle

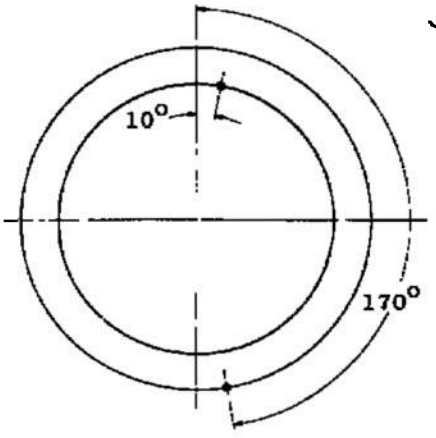

d. Station 2C

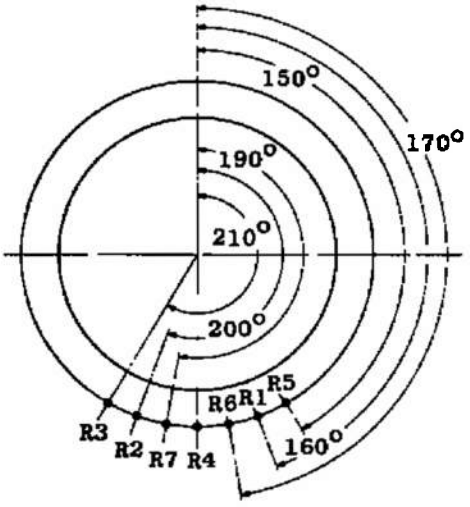

e. Station R1 – R7

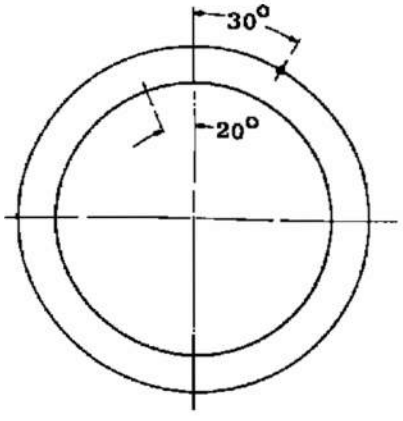

f. Station 3A

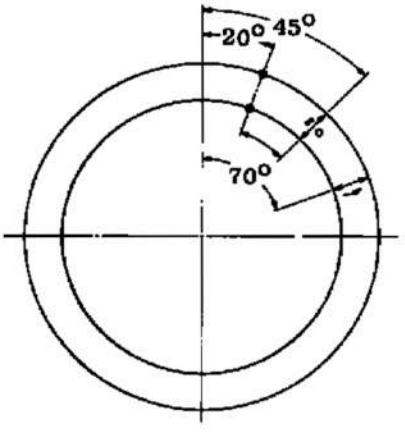

g. Station 3B

Fig. 11 Continued

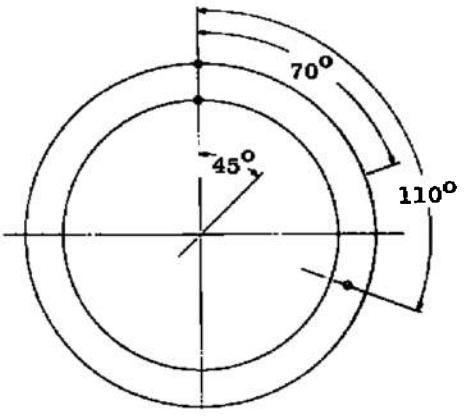

h. Station 3C

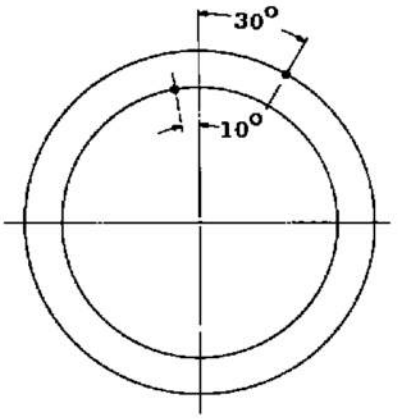

i. Station 3D

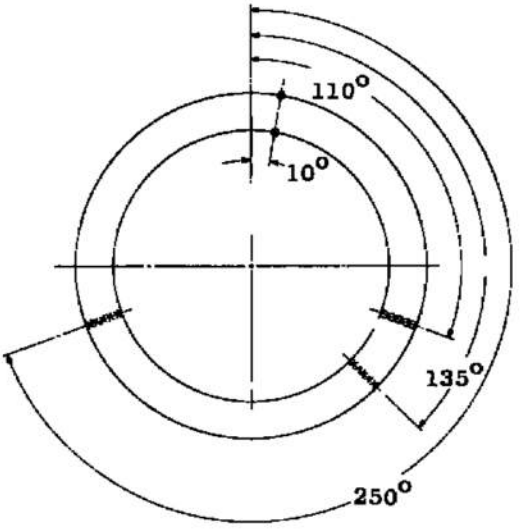

j. Station 3E

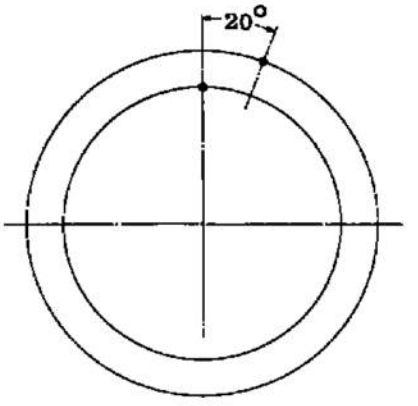

k. Station 3F

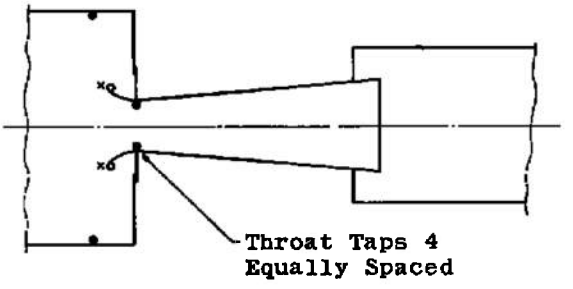

l. Venturi Instrumentation

Fig. 11 Concluded

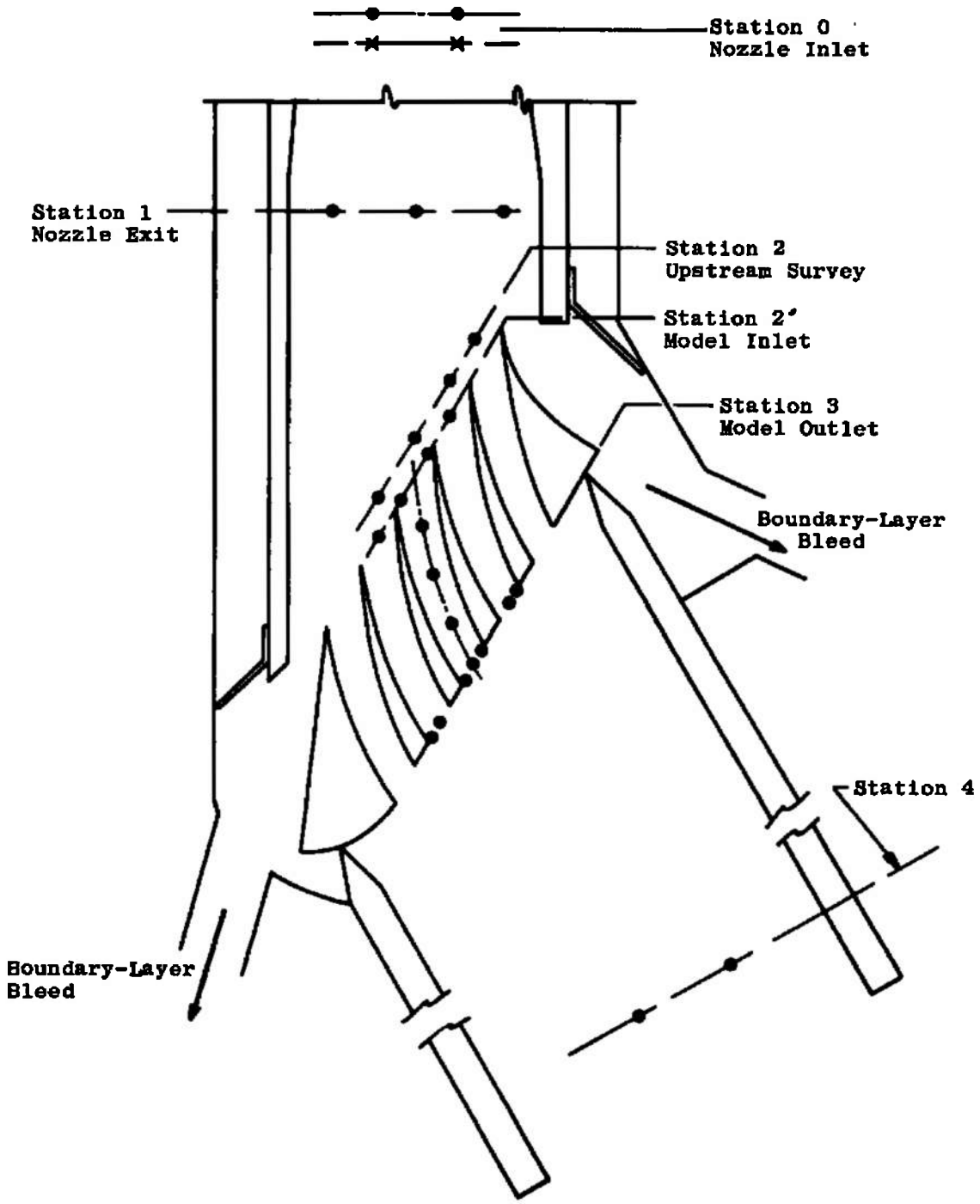

Fig. 12 Details of Cascade Rig Instrumentation

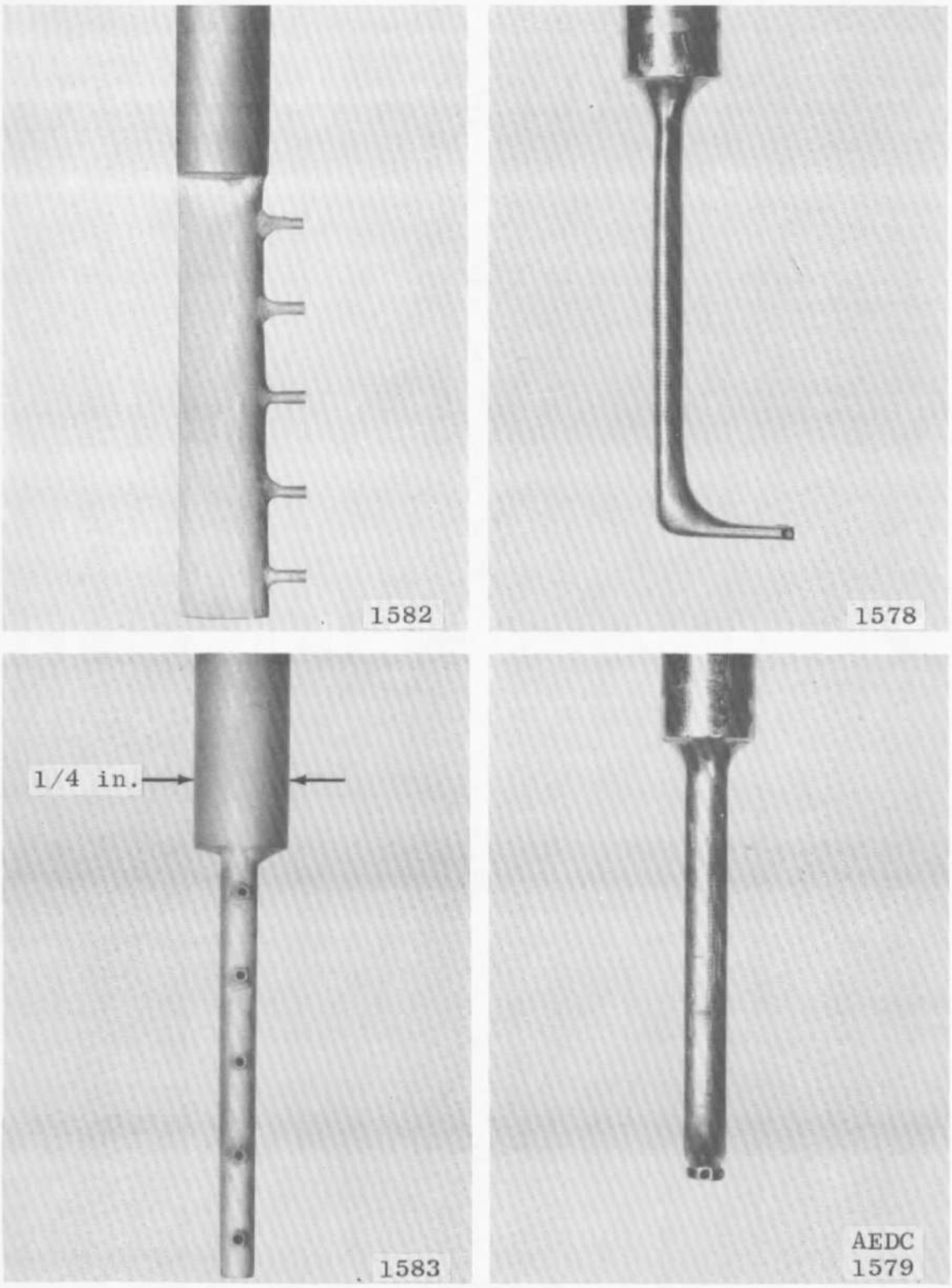

(a) (b)

Fig. 13 Aerodynamic Instrumentation

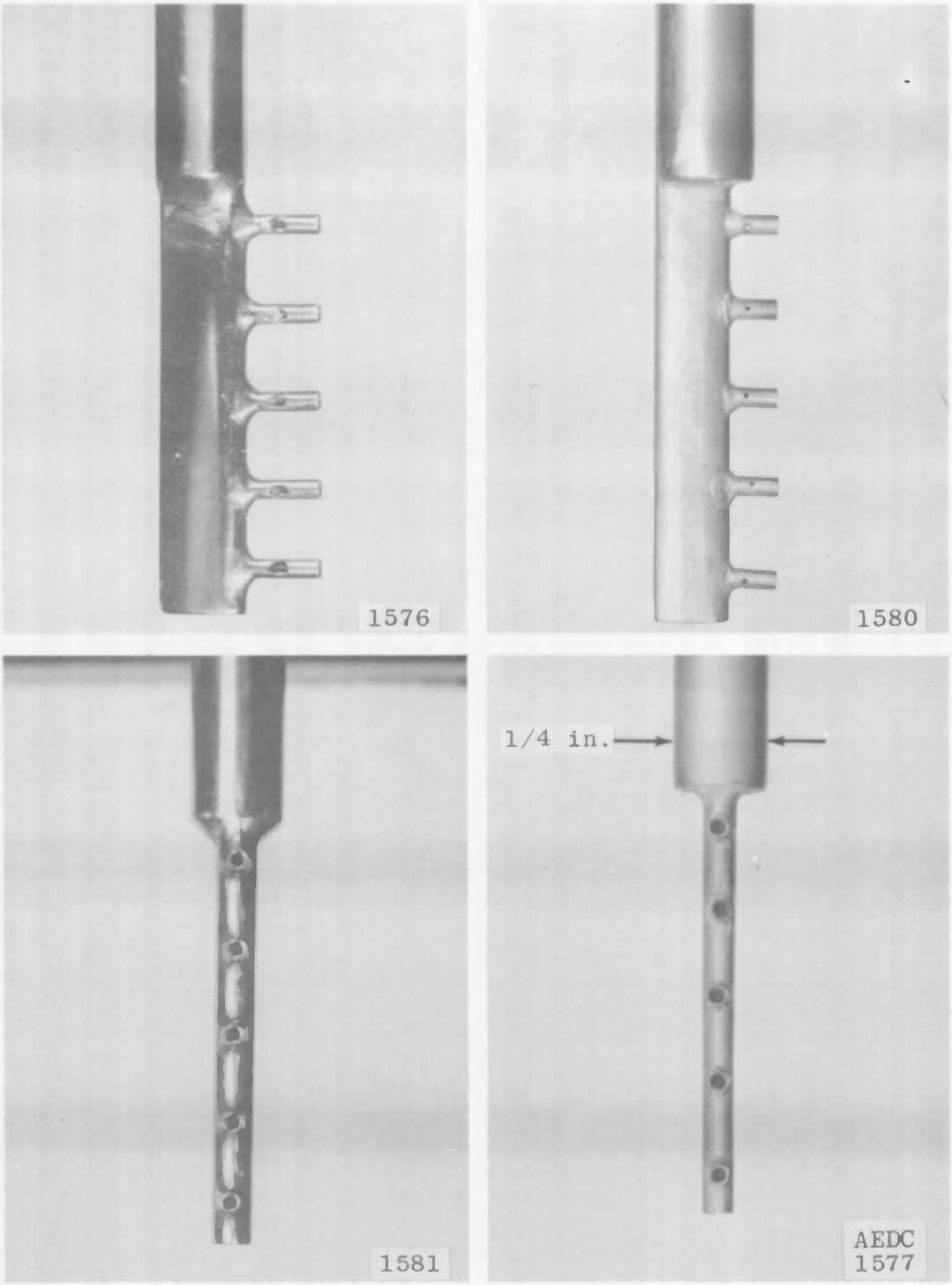

(c) (d)

Fig. 13 Continued

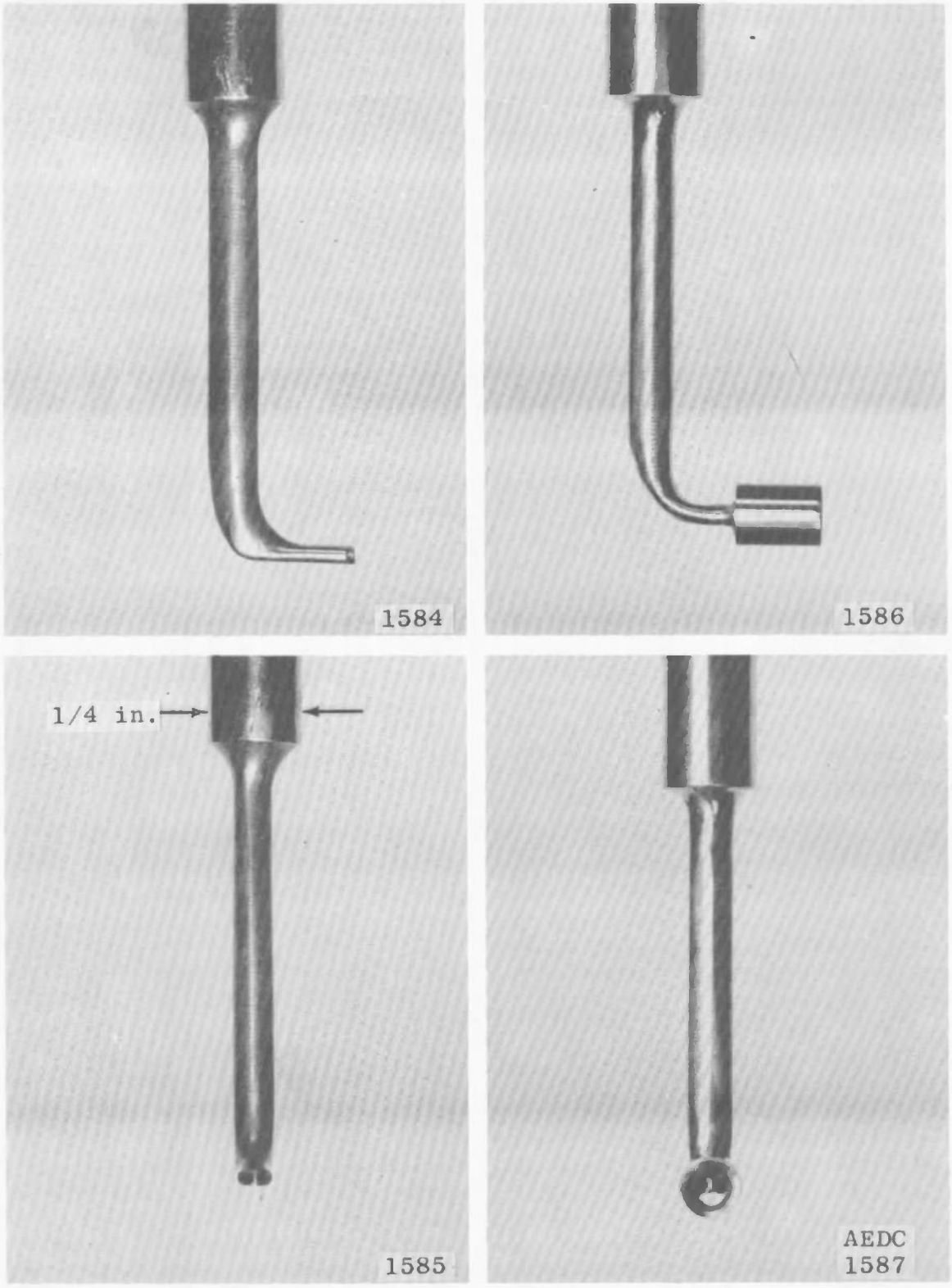

(e) (f)

Fig. 13 Concluded

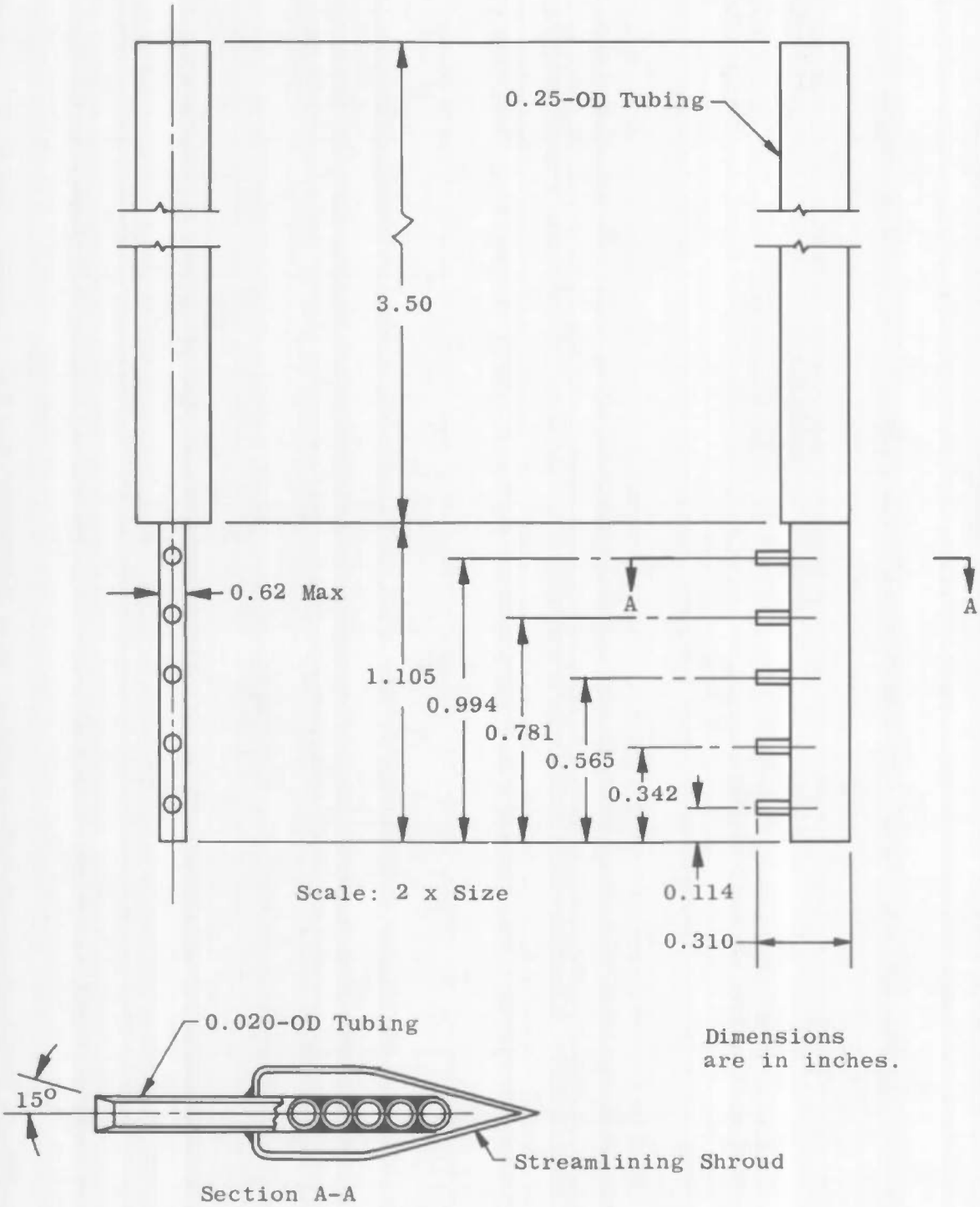

a. Conical Inlet Total Pressure Rake

Fig. 14 Design Details of Probes

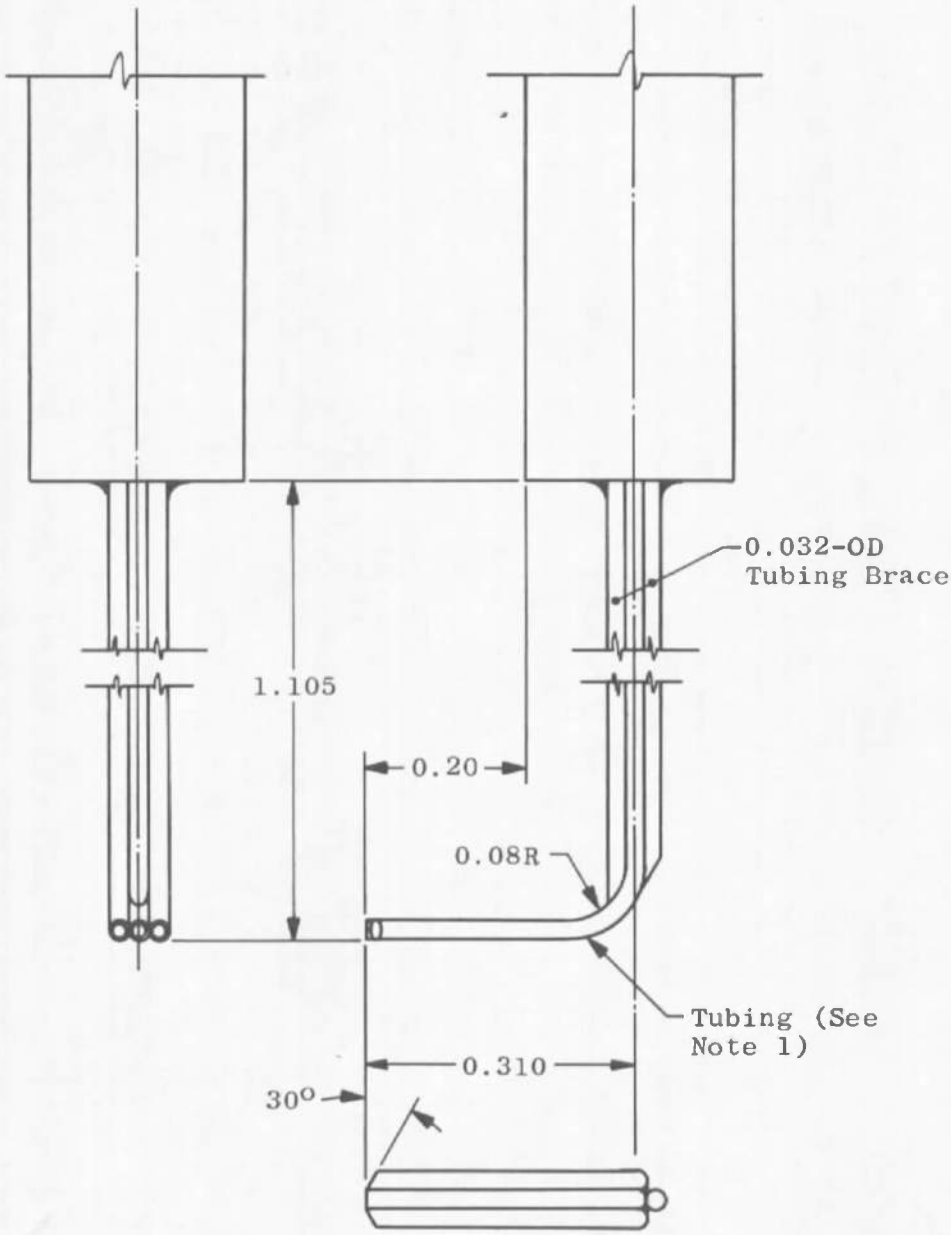

Notes: 1. These probes are made with 0.020-, 0.040-, and 0.060-OD tubes. The probe shown has 0.020-OD tubes.
2. Dimensions are in inches.

b. Combined Yaw and Total Pressure Probes

Fig. 14 Continued

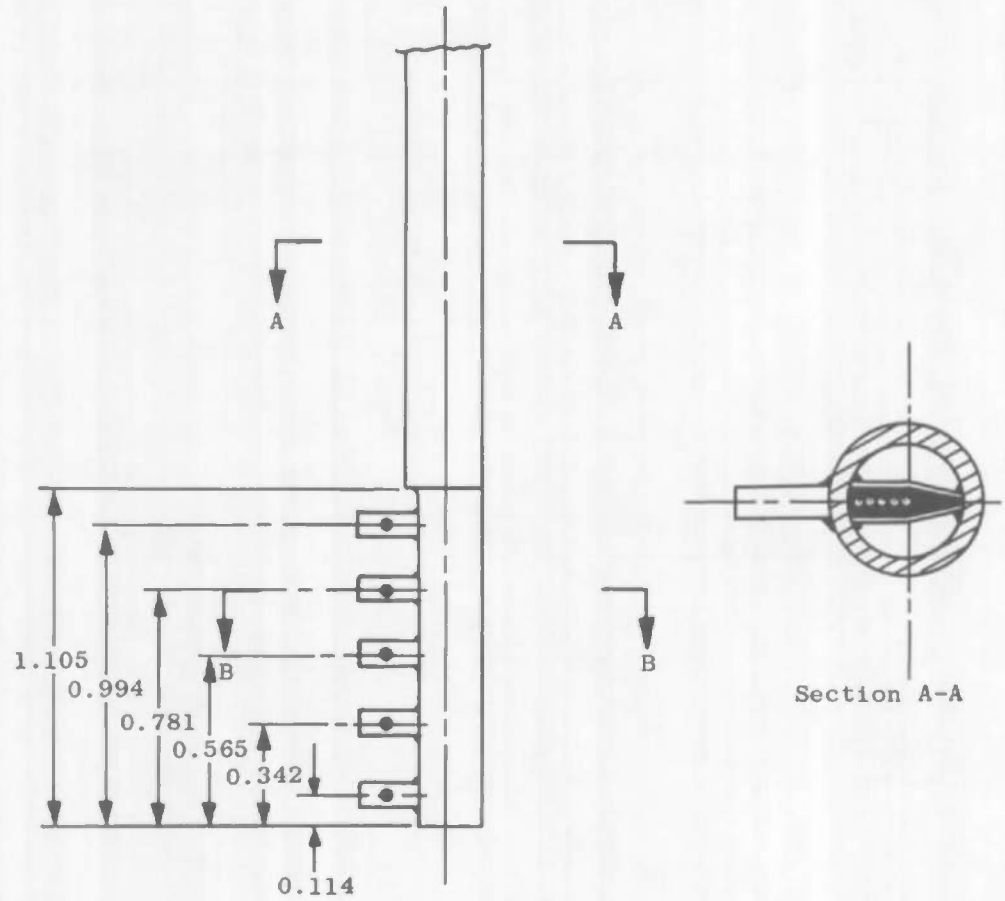

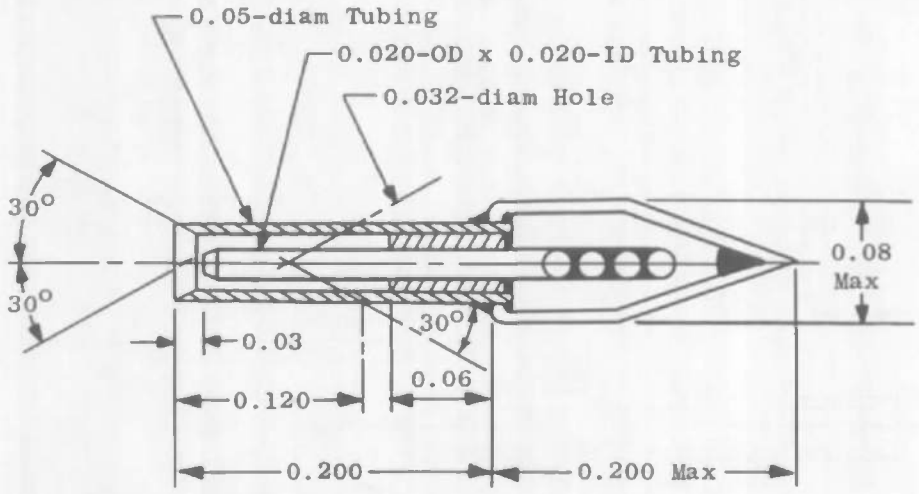

Dimensions are in inches.

Section B-B

c. Total Pressure Rake

Fig. 14 Continued

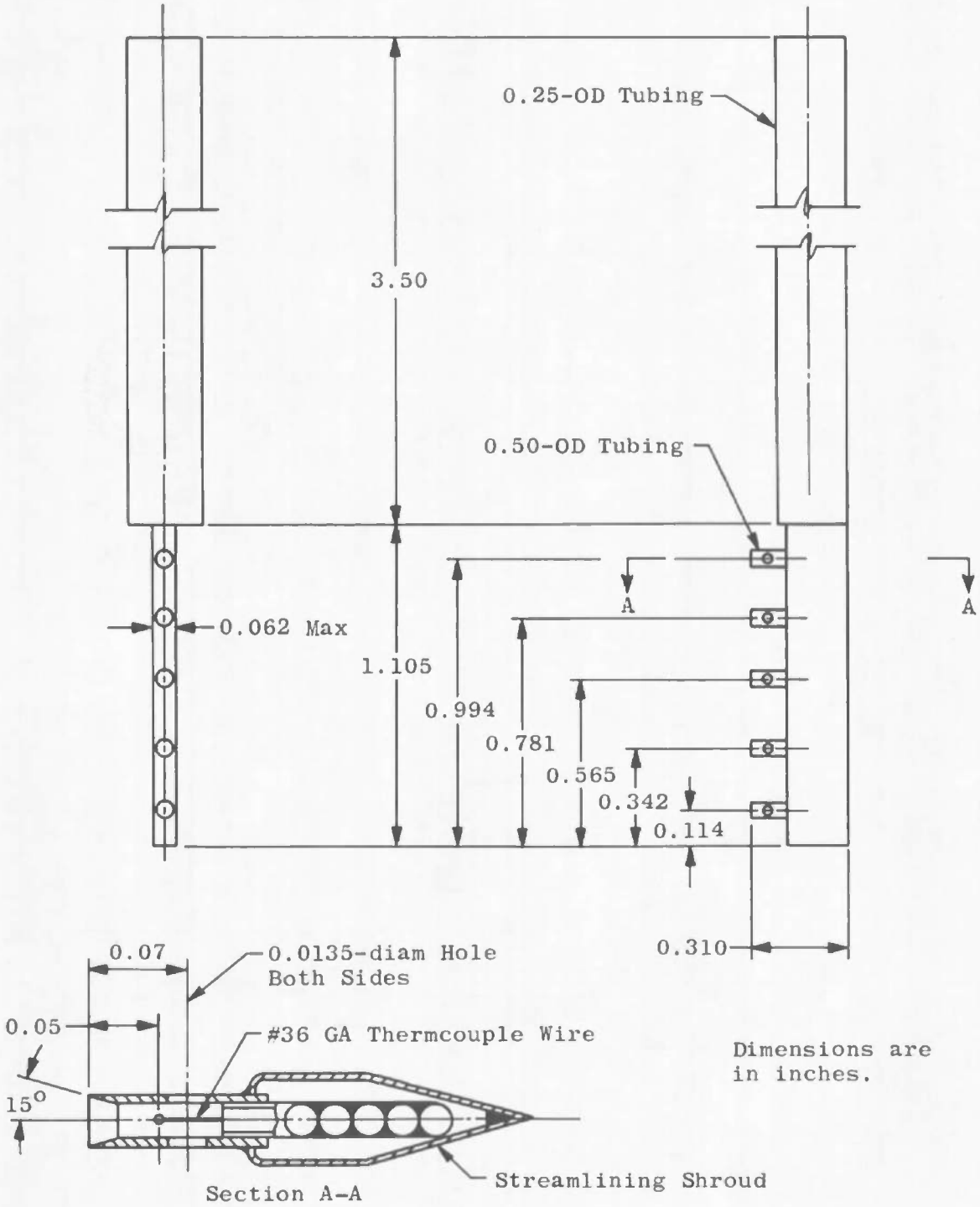

d. Thermocouple Rake

Fig. 14 Continued

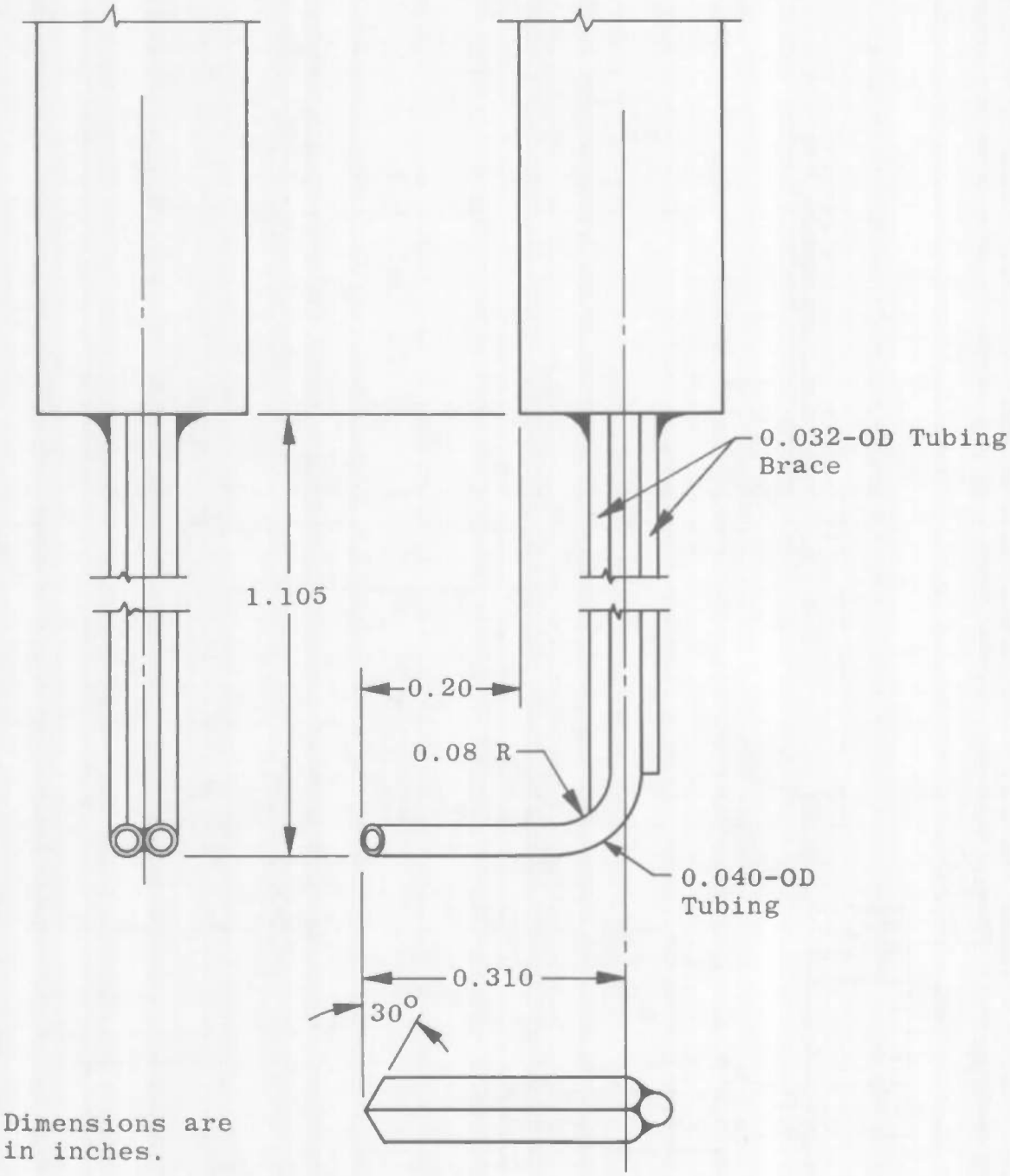

e. Yaw Probe

Fig. 14 Continued

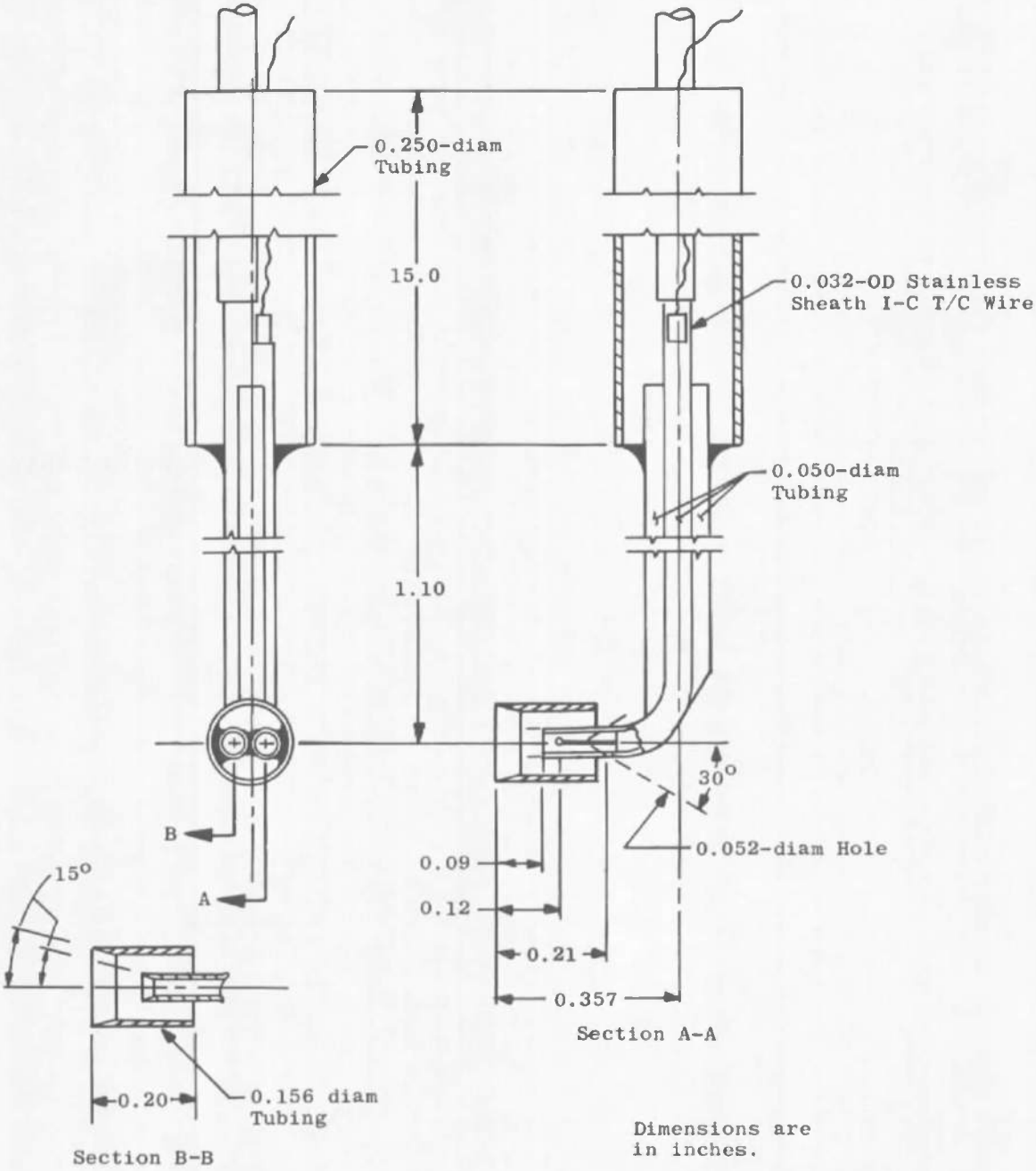

f. Total Temperature and Pressure Probe

Fig. 14 Concluded

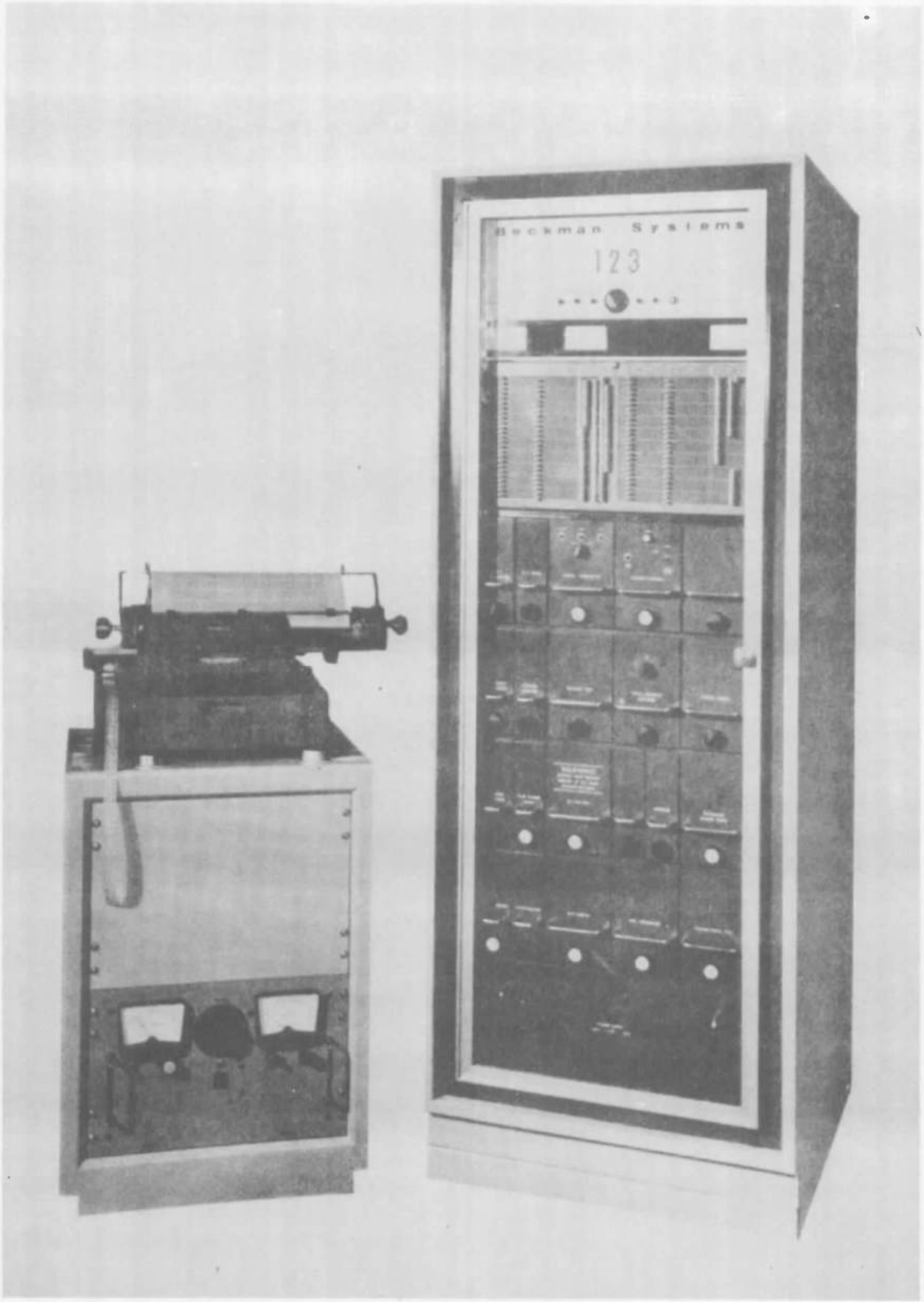

Fig. 15 Data Processing System Model 123

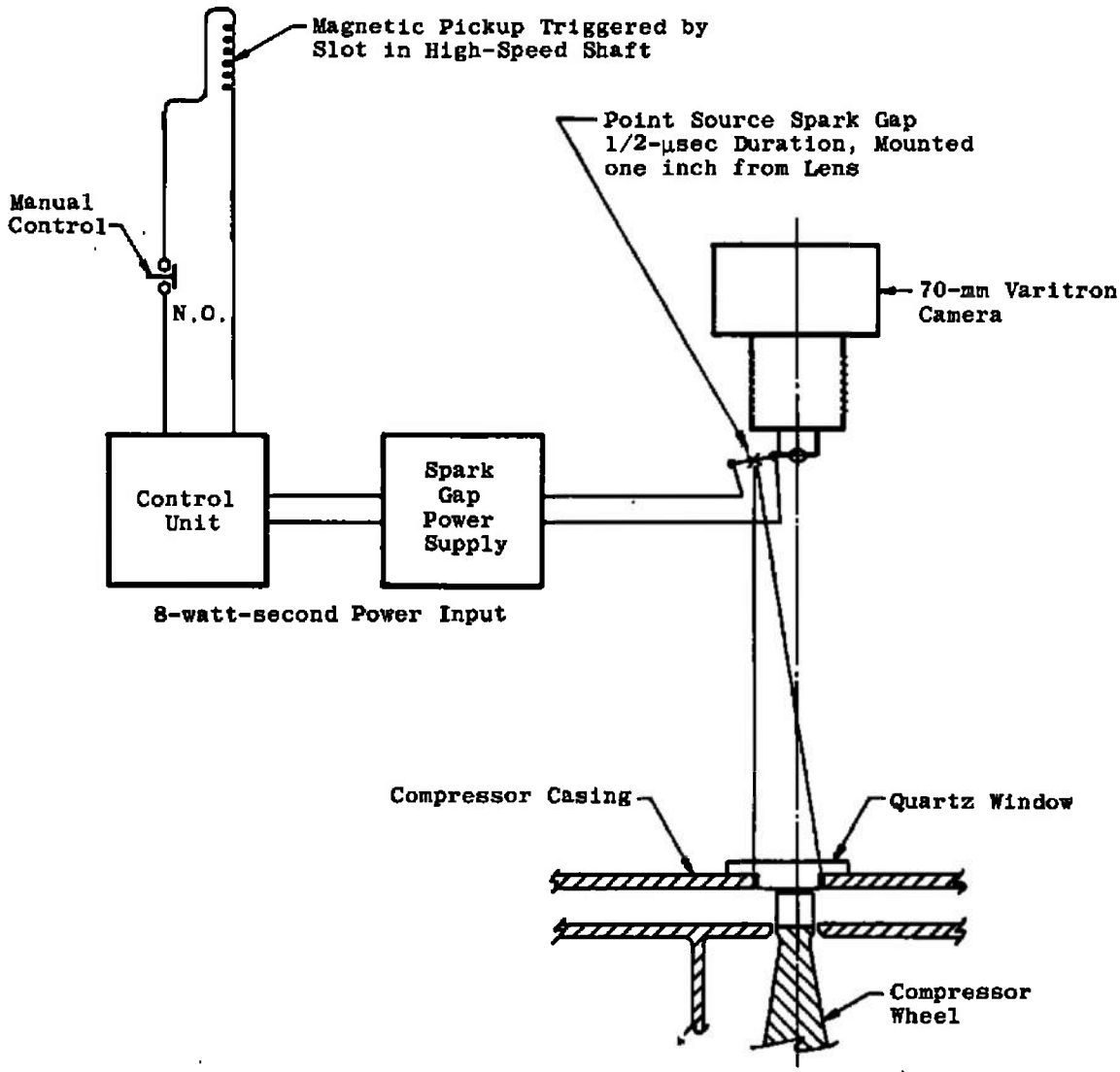

Fig. 16 Shadowgraph Apparatus

TABLE I
COMPRESSOR TEST RIG INSTALLATION

Parameter	Measuring Device	Range	Primary Recording Method	Estimated System Accuracy
Compressor and Venturi Inlet Temperatures	Iron-Constantan Thermocouples	30-150°F	Analog-to-digital Converter	± 1°F
Compressor Discharge Temperature	Iron-Constantan Thermocouples	50-400°F	Analog-to-digital Converter	± 1°F
Compressor Inlet Total and Static Pressures	Strain-Gage Transducers	± 5 psid	Analog-to-digital Converter	± 2%
Rotor Wall Static Pressure	Strain-Gage Transducers	± 25 psid	Analog-to-digital Converter	± 2%
Compressor Discharge Total and Static and Venturi Inlet Pressures	Strain-Gage Transducers	50 psia	Analog-to-digital Converter	± 1/4%
Venturi Throat Static Pressure	Strain-Gage Transducers	15 psia	Analog-to-digital Converter	± 1%

TABLE I (Concluded)

Parameter	Measuring Device	Range	Primary Recording Method	Estimated System Accuracy
Compressor Rotor Speed	Magnetic Pulse Pickup	0-21,000 cps	Event-per-unit-time Counter	± 1 count
Compressor Inlet and Outlet Flow Angle	Yaw Probe & Null-Balance Transducer	-90 to +90°	Remote operated angle actuator and potentiometer type. strip chart recorder	± 1°
Torque Force	Phase-Shift Torquemeter	0-10,000 in.-lb	Analog-to-digital Converter	± 2% above 3000 in.-lb, ±5% in 0-3000 in.-lb range
Lube Oil Pressures	Bourdon Tube Gage	0-100 psig	Remote Synchro Gage	± 10%
Oil and Bearing Temperatures	Copper-Constantan Thermocouples	-100 to +400°F	Temperature-compensated Millivolt Indicator	± 10%
Vibration Amplitude and Velocity	Velocity Pickups	0-5 mils	Millivolt Indicator	± 2%

UNCLASSIFIED

Security Classification

DOCUMENT CONTROL DATA - R&D

(Security classification of title, body of abstract and indexing annotation must be entered when the overall report is classified)

1. ORIGINATING ACTIVITY (Corporate author)
Arnold Engineering Development Center
ARO, Inc.
Arnold Air Force Station, Tennessee

2a. REPORT SECURITY CLASSIFICATION
UNCLASSIFIED

2b. GROUP

3. REPORT TITLE
DEVELOPMENT OF THE SUPERSONIC COMPRESSOR TEST FACILITIES AT THE ARNOLD ENGINEERING DEVELOPMENT CENTER

4. DESCRIPTIVE NOTES (Type of report and inclusive dates)

5. AUTHOR(S) (Last name, first name, initial)
Carman, C. T., ARO, Inc.

6. REPORT DATE
October 1965

7a. TOTAL NO. OF PAGES
83

7b. NO. OF REFS
6

8a. CONTRACT OR GRANT NO. AF 40(600)-1200

b. PROJECT NO. 7065

c. Program Element 61445014

d. Task 706501

9a. ORIGINATOR'S REPORT NUMBER(S)
AEDC-TR-65-169

9b. OTHER REPORT NO(S) (Any other numbers that may be assigned this report)

10. AVAILABILITY/LIMITATION NOTICES
Qualified requesters may obtain copies of this report from DDC.

11. SUPPLEMENTARY NOTES

12. SPONSORING MILITARY ACTIVITY
Arnold Engineering Development Center
Air Force Systems Command
Arnold Air Force Station, Tennessee

13. ABSTRACT

The design characteristics, operational capabilities, and instrumentation systems of the supersonic compressor test facilities at AEDC are described and the results of shakedown tests are presented. These facilities consist of (1) a high-speed rotating machine to test 22-in.-diam, single-stage, axial-flow compressor rotors from 5,000 to 17,000 rpm at rotor tip speeds up to 1630 ft/sec and (2) a continuous-flow cascade rig with a 1- by 1.3-in. test section to test the effects of various blade parameters such as area ratio and angle of attack. The primary purpose of these facilities is for further development and evaluation of the concept of blunt-trailing edge, supersonic compressor blades.

This document ... proved for public release ... its distribution is unlimited. Per DDC TR-75-5 AD-A011 100 Dtd July, 1975

DD FORM 1 JAN 64 1473

UNCLASSIFIED

Security Classification

14 KEY WORDS	LINK A ROLE	LINK A WT	LINK B ROLE	LINK B WT	LINK C ROLE	LINK C WT
test facilities						
supersonic compressors						
axial-flow compressors						
design						
operation						
instrumentation systems						
cascade rigs						
blunt-trailing-edge blades						

INSTRUCTIONS

1. ORIGINATING ACTIVITY: Enter the name and address of the contractor, subcontractor, grantee, Department of Defense activity or other organization *(corporate author)* issuing the report.

2a. REPORT SECURITY CLASSIFICATION: Enter the overall security classification of the report. Indicate whether "Restricted Data" is included. Marking is to be in accordance with appropriate security regulations.

2b. GROUP: Automatic downgrading is specified in DoD Directive 5200.10 and Armed Forces Industrial Manual. Enter the group number. Also, when applicable, show that optional markings have been used for Group 3 and Group 4 as authorized.

3. REPORT TITLE: Enter the complete report title in all capital letters. Titles in all cases should be unclassified. If a meaningful title cannot be selected without classification, show title classification in all capitals in parenthesis immediately following the title.

4. DESCRIPTIVE NOTES: If appropriate, enter the type of report, e.g., interim, progress, summary, annual, or final. Give the inclusive dates when a specific reporting period is covered.

5. AUTHOR(S): Enter the name(s) of author(s) as shown on or in the report. Enter last name, first name, middle initial. If military, show rank and branch of service. The name of the principal author is an absolute minimum requirement.

6. REPORT DATE: Enter the date of the report as day, month, year; or month, year. If more than one date appears on the report, use date of publication.

7a. TOTAL NUMBER OF PAGES: The total page count should follow normal pagination procedures, i.e., enter the number of pages containing information.

7b. NUMBER OF REFERENCES: Enter the total number of references cited in the report.

8a. CONTRACT OR GRANT NUMBER: If appropriate, enter the applicable number of the contract or grant under which the report was written.

8b, 8c, & 8d. PROJECT NUMBER: Enter the appropriate military department identification, such as project number, subproject number, system numbers, task number, etc.

9a. ORIGINATOR'S REPORT NUMBER(S): Enter the official report number by which the document will be identified and controlled by the originating activity. This number must be unique to this report.

9b. OTHER REPORT NUMBER(S): If the report has been assigned any other report numbers *(either by the originator or by the sponsor)*, also enter this number(s).

10. AVAILABILITY/LIMITATION NOTICES: Enter any limitations on further dissemination of the report, other than those imposed by security classification, using standard statements such as:

(1) "Qualified requesters may obtain copies of this report from DDC."

(2) "Foreign announcement and dissemination of this report by DDC is not authorized."

(3) "U. S. Government agencies may obtain copies of this report directly from DDC. Other qualified DDC users shall request through _____."

(4) "U. S. military agencies may obtain copies of this report directly from DDC. Other qualified users shall request through _____."

(5) "All distribution of this report is controlled. Qualified DDC users shall request through _____."

If the report has been furnished to the Office of Technical Services, Department of Commerce, for sale to the public, indicate this fact and enter the price, if known.

11. SUPPLEMENTARY NOTES: Use for additional explanatory notes.

12. SPONSORING MILITARY ACTIVITY: Enter the name of the departmental project office or laboratory sponsoring *(paying for)* the research and development. Include address.

13. ABSTRACT: Enter an abstract giving a brief and factual summary of the document indicative of the report, even though it may also appear elsewhere in the body of the technical report. If additional space is required, a continuation sheet shall be attached.

It is highly desirable that the abstract of classified reports be unclassified. Each paragraph of the abstract shall end with an indication of the military security classification of the information in the paragraph, represented as *(TS)*, *(S)*, *(C)*, or *(U)*.

There is no limitation on the length of the abstract. However, the suggested length is from 150 to 225 words.

14. KEY WORDS: Key words are technically meaningful terms or short phrases that characterize a report and may be used as index entries for cataloging the report. Key words must be selected so that no security classification is required. Identifiers, such as equipment model designation, trade name, military project code name, geographic location, may be used as key words but will be followed by an indication of technical context. The assignment of links, rules, and weights is optional.